

Environmental Science Atmospheres

Accepted Manuscript

This article can be cited before page numbers have been issued, to do this please use: A. Akherati, Y. He, L. A. Garofalo, A. L. Hodshire, D. Farmer, S. M. Kreidenweis, W. Pernar, L. Hu, E. V. Fischer, C. N. Jen, A. Goldstein, E. J. T. Levin, P. DeMott, T. L. Campos, F. Flocke, J. M. Reeves, D. W. Toohey, J. R. Pierce and S. Jathar, *Environ. Sci.: Atmos.*, 2022, DOI: 10.1039/D1EA00082A.



This is an Accepted Manuscript, which has been through the Royal Society of Chemistry peer review process and has been accepted for publication.

Accepted Manuscripts are published online shortly after acceptance, before technical editing, formatting and proof reading. Using this free service, authors can make their results available to the community, in citable form, before we publish the edited article. We will replace this Accepted Manuscript with the edited and formatted Advance Article as soon as it is available.

You can find more information about Accepted Manuscripts in the [Information for Authors](#).

Please note that technical editing may introduce minor changes to the text and/or graphics, which may alter content. The journal's standard [Terms & Conditions](#) and the [Ethical guidelines](#) still apply. In no event shall the Royal Society of Chemistry be held responsible for any errors or omissions in this Accepted Manuscript or any consequences arising from the use of any information it contains.

Environmental Significance Statement

Wildfires are an important atmospheric source of primary organic aerosol (POA) and precursors for secondary organic aerosol (SOA) at regional and global scales. However, there are large uncertainties surrounding the emissions and physicochemical processes that control the transformation, evolution, and properties of POA and SOA in large wildfire plumes. In this work, we develop a plume version of a kinetic model to simulate the dilution, oxidation chemistry, thermodynamic properties, and microphysics of organic aerosol (OA) in wildfire smoke. We find that dilution-driven evaporation of POA and simultaneous photochemical production of SOA are likely to explain the observed evolution of OA in wildfire plumes. Further, we show that there is rapid chemical transformation of wildfire smoke aerosol within the first hour after emission, driven by high concentrations of the hydroxyl radical.



1 Dilution and Photooxidation Driven Processes Explain the Evolution of 2 Organic Aerosol in Wildfire Plumes

3 Ali Akherati¹*, Yicong He¹, Lauren A. Garofalo², Anna L. Hodshire², Delphine K. Farmer², Sonia M.
4 Kreidenweis³, Wade Permar⁴, Lu Hu⁴, Emily V. Fischer³, Coty N. Jen⁵, Allen H. Goldstein⁶, Ezra J. T.
5 Levin³, Paul J DeMott³, Teresa L. Campos⁷, Frank Flocke⁷, John M. Reeves⁷, Darin W. Toohey⁸, Jeffrey
6 R. Pierce^{3*}, and Shantanu H. Jathar^{1*}

7 ¹Department of Mechanical Engineering, Colorado State University, Fort Collins, CO, USA

8 ²Department of Chemistry, Colorado State University, Fort Collins, CO, USA

9 ³Department of Atmospheric Science, Colorado State University, Fort Collins, CO, USA

10 ⁴Department of Chemistry and Biochemistry, University of Montana, Missoula, MT, USA

11 ⁵Department of Chemical Engineering, Carnegie Mellon University, Pittsburgh, PA, USA

12 ⁶Department of Environmental Science, Policy & Management, University of California Berkeley,
Berkeley, CA, USA

13 ⁷Earth Observing Laboratory, National Center for Atmospheric Research, Boulder, CO, USA

14 ⁸Department of Atmospheric and Oceanic Science, University of Colorado Boulder, Boulder, CO, USA

15 *Correspondence to: Shantanu H. Jathar (shantanu.jathar@colostate.edu) and Jeffrey R. Pierce
(jeffrey.pierce@colostate.edu)

16 Now at the Department of Civil and Environmental Engineering, University of California Davis, Davis,
CA, USA

21 Abstract

22 Wildfires are an important atmospheric source of primary organic aerosol (POA) and precursors
23 for secondary organic aerosol (SOA) at regional and global scales. However, there are large uncertainties
24 surrounding the emissions and physicochemical processes that control the transformation, evolution, and
25 properties of POA and SOA in large wildfire plumes. We develop a plume version of a kinetic model to
26 simulate the dilution, oxidation chemistry, thermodynamic properties, and microphysics of organic
27 aerosol (OA) in wildfire smoke. The model is applied to study the in-plume OA in four large wildfire
28 smoke plumes intercepted during an aircraft-based field campaign in summer 2018 in the western United
29 States. Based on estimates of dilution and oxidant concentrations before the aircraft first intercepted the
30 plumes, we simulate the OA evolution from very close to the fire to several hours downwind. Our model
31 results and sensitivity simulations suggest that dilution-driven evaporation of POA and simultaneous
32 photochemical production of SOA are likely to explain the observed evolution in OA mass with physical
33 age. The model, however, substantially underestimates the change in the oxygen-to-carbon ratio of the
34 OA compared to measurements. In addition, we show that the rapid chemical transformation within the
35 first hour after emission is driven by higher-than-ambient OH concentrations (3×10^6 - 10^7 molecules cm^{-3})
36 and the slower evolution over the next several hours is a result of lower-than-ambient OH concentrations
37 ($< 10^6$ molecules cm^{-3}) and depleted SOA precursors. Model predictions indicate that the OA measured
38 several hours downwind of the fire is still dominated by POA but with an SOA fraction that varies
39 between 30% and 56% of the total OA. Semivolatile, heterocyclic, and oxygenated aromatic compounds,
40 in that order, were found to contribute substantially (>90%) to SOA formation. Future work needs to
41 focus on better understanding the dynamic evolution closer to the fire and resolving the rapid change in
42 the oxidation state of OA with physical age.

43 1. Introduction

44 Wildfires are an important source of organic aerosol (OA) and OA precursors to the
45 atmosphere.¹⁻⁶ Wildfire OA, as a major component of the submicron atmospheric aerosol mass,^{7,8} has
46 been estimated to exert a strong influence on the Earth's radiative budget,^{9,10} and adversely affect regional
47 and global air quality,^{8,11-13} human health,^{14,15} and visibility.^{14,16} Yet, there are large uncertainties
48 surrounding the emissions and processes that control the abundance, distribution, and properties of
49 wildfire OA in the atmosphere. For example, primary emissions of biomass burning OA, which includes



51 OA from wildfires, agricultural fires, and biofuel combustion, vary by a factor of 2 in published
52 inventories¹⁷ while atmospheric production rates of biomass burning OA, have been shown to vary over
53 two orders of magnitude in several recent global modeling studies (1-100 Tg yr⁻¹).¹⁸ These uncertainties
54 have made it extremely challenging to represent wildfire OA in large-scale atmospheric models, which, in
55 part, have limited the ability of these models to predict the atmospheric and environmental impacts of
56 wildfire emissions.

57 Wildfires directly emit particles that are dominated by primary organic aerosol (POA) with
58 smaller amounts of black carbon (BC) and inorganic species (e.g., sulfate, nitrate, potassium).^{4,19,20}
59 Wildfire POA has been shown to be semivolatile and evaporates with dilution.²¹⁻²³ Furthermore, wildfire
60 POA and the vapors in equilibrium with the POA (or semivolatile organic compounds, SVOC) are also
61 known to be reactive²³⁻²⁵. Wildfires emit OA precursors that include intermediate-volatility and volatile
62 organic compounds (IVOC and VOC)²⁶⁻²⁸ and these oxidize in the atmosphere to form secondary organic
63 aerosol (SOA).²⁹ In addition to emissions of reduced hydrocarbons such as alkanes, aromatic, and
64 biogenic VOCs,⁴ wildfires also emit oxygenated IVOCs and VOCs.^{23,27,28,30-34} These include oxygenated
65 aromatic and heterocyclic organic compounds that have recently been shown to be important precursors
66 for SOA formation.³⁵⁻³⁹ Although a lot has been understood about the composition, oxidation chemistry,
67 and properties of OA and OA precursors from biomass burning emissions, especially in laboratory
68 experiments, a detailed understanding of the physicochemical evolution of OA and OA precursors in real
69 wildfire plumes is less well understood.

70 Recently, Hodshire et al.⁴⁰ undertook a comprehensive review of wildfire OA data gathered in
71 four laboratory campaigns and thirteen field campaigns performed over the past two decades. An analysis
72 of these data suggested that while photooxidation of biomass burning emissions resulted in an
73 enhancement in OA mass in laboratory experiments (mean=1.25, median=1.44, and interquartile range or
74 IQR=1.1-1.54),^{37-39,41-43} a similar enhancement was missing for the OA tracked in real wildfire plumes
75 (mean=1.1, median=1.0, and IQR=0.77-1.0).^{20,44-60} In addition, the OA measured within wildfire plumes
76 closest to the fire (<1 hr) was more oxidized (i.e., a higher oxygen-to-carbon (O:C) ratio for the OA)
77 (mean=0.36, median=0.38, and IQR=0.18-0.54) than the initial OA measured in laboratory experiments
78 (mean=0.23, median=0.23, and IQR=0.17-0.29), and the OA from wildfires exhibited a stronger O:C
79 enhancement with photochemical age (mean=1.82, median=1.85, and IQR=1.5-2.0) than the OA from
80 laboratory fires (mean=1.6, median=1.5, and IQR=1.3-1.8). Similar to the trends in OA O:C, a different
81 enhancement was also observed for the ratio of two mass fragments (m_{44}/m_{60}) measured by the aerosol
82 mass spectrometer between the field (mean=4.5, median=3.8, and IQR=2.3-6.7) and the laboratory
83 (mean=3.5, median=3.0 and IQR=1.8-3.6). m_{44} refers to the mass fragment that is associated with the
84 low-volatility organic compounds found in SOA⁶¹ while m_{60} refers to the mass fragment arising from
85 fragmentation of primary emissions of anhydrous sugars such as levoglucosan.⁵⁴

86 Based on this analysis, Hodshire et al.⁴⁰ put forth four hypotheses to explain this field versus
87 laboratory difference. First, they argued that the dilution of the wildfire plume could result in evaporation
88 of POA and this evaporation could be approximately balanced by SOA production to result in a small
89 change in the OA mass with photochemical aging. Since the condensing SOA is likely to have a higher
90 O:C ratio than the evaporating POA, this POA-SOA swap would not affect the OA mass but instead
91 produce an increase in the O:C ratio with aging. This hypothesis has been supported by theoretical
92 calculations.^{62,63} Second, the authors hypothesized that because wildfire plumes are typically only
93 sampled at least 15 minutes after emission (often longer), the plume measurements could have missed the
94 OA evolution that happened prior to the first measurement. Early sampling poses safety issues as well as
95 the prospect of measuring poorly mixed plumes. If rapid chemistry does indeed occur early on, this may
96 explain both the higher O:C ratio measured in the field and the reduced propensity to form SOA after the
97 aircraft first intercepts a plume. Third, they postulated that the field and laboratory differences could arise
98 from differences in the emissions and chemistry of OA and OA precursors, attributed to differences in the
99 fuel mixtures, burn conditions, combustion efficiency, and environmental conditions (e.g., temperature,
100 relative humidity) and regimes (e.g., photolytic rates, NO_x). Finally, they noted several experimental
101 artifacts linked to laboratory experiments, including losses of OA and OA precursors to transfer ducts³⁸



102 and walls of the environmental chamber,^{64–66} that could drive differences between laboratory and field
103 measurements. For the most part, these hypotheses remain untested and will serve as the basis for this
104 work.

105 Several studies have tested the first hypothesis above, i.e. that dilution-driven evaporation of POA
106 is roughly balanced by SOA production in wildfire plumes.^{33,67} In one of these studies based on wildfire
107 plumes sampled in the western United States (US), Palm et al.³³ quantified the evolution of OA mass as a
108 function of dilution and photochemical age. They found that plumes that had diluted but not yet
109 undergone photooxidation showed evidence for POA evaporation, while plumes that had both diluted and
110 undergone photooxidation showed evidence for replacement of the lost POA mass with SOA. However,
111 Palm et al.³³ did not account for the photochemical evolution prior to the first sample (i.e. < 30 minutes
112 since emission), nor did they account for the oxidation of all potential precursors (i.e., SVOCs) leading to
113 SOA formation. Based on closure calculations, they argued that nearly 90% of the SOA came from
114 oxidation of evaporated POA vapors with marginal contributions from other VOCs. To the best of our
115 knowledge, no bottom-up, detailed models have been used to simulate and evaluate the OA mass and
116 composition evolution in wildfire plumes.

117 In this study, we simulated the physicochemical evolution of OA in a subset of wildfire plumes
118 sampled during a recent airborne field campaign based in the western US. The OA evolution was
119 simulated using a kinetic model that accounts for the dilution, oxidation chemistry, thermodynamic
120 properties, and microphysics of OA. A novel contribution of this work is that we incorporate estimates of
121 dilution and photochemical age before the first airborne plume transect, to simulate the OA evolution
122 from very close to the fire to several hours downwind. Model results of mass and composition were
123 compared to plume measurements to study the contribution of precursors and processes to OA evolution.

125 2. Materials and Methods

126 2.1 Aircraft Measurements

127 The analysis in this work is centered around measurements made during the Western Wildfire
128 Experiment for Cloud Chemistry, Aerosol Absorption, and Nitrogen (WE-CAN) field campaign. An
129 extensive description of the field campaign and instrumentation used can be found in Lindaas et al.⁶⁸ and
130 Juncosa Calahorrano et al.⁶⁹ Briefly, during WE-CAN, the NSF/NCAR C-130 research aircraft was
131 deployed between July and September 2018 to sample the evolution of trace gases and particles in
132 wildfire smoke plumes over the western US. Smoke was sampled from 23 distinct wildfires over this
133 period and for 12 of these wildfires, the aircraft was flown along horizontal transects orthogonal to the
134 wind direction to perform pseudo-Lagrangian sampling of plumes. Multiple transects (4 to 14 per fire)
135 were executed along the length of the wildfire plume over multiple hours (2 to 6 hours of physical age)
136 and several hundred kilometers from the source of the fire (10 to 220 km). We should note that near-
137 Lagrangian sampling was accomplished for only a few of the wildfire plumes (e.g., Taylor Creek, later
138 transects for Sharps) and, in most cases, the sampling was pseudo-Lagrangian. As shown in Figure S1,
139 the aircraft sampled much faster (twice as fast, on average) than the physical age of the plume for four out
140 of the five transect sets studied in this work. The modeling and analysis undertaken in this work assumes
141 that the fuel and burn conditions and, therefore, the emissions remained constant during the measurement
142 time period. In other words, we assumed that the measurements represent a true Lagrangian dataset and
143 this assumption should be considered while interpreting the results. In addition to performing transects
144 through the center/core of the wildfire plume, for some wildfire plumes the aircraft also performed
145 transects at different altitudes to probe vertical variability in composition and environmental conditions.
146 These data were excluded from the analysis presented in this work.

147 Here, we focused on the evolution of the smoke emitted from the following four wildfires: Taylor
148 Creek Fire (southwest Oregon), Sharps Fire (southern Idaho), Bear Trap Fire (eastern Utah), and Silver
149 Creek Fire (northwest Colorado). The aircraft completed two distinct pseudo-Lagrangian sampling efforts
150 for the Bear Trap Fire and each of these transect sets were analyzed separately. In total, the analysis
151 focused on five transect sets. The location and dominant fuel(s) for each wildfire can be found in Table 1
152 of Lindaas et al.⁶⁸ These wildfires were chosen because of their ideal sampling strategy, clear trends in the

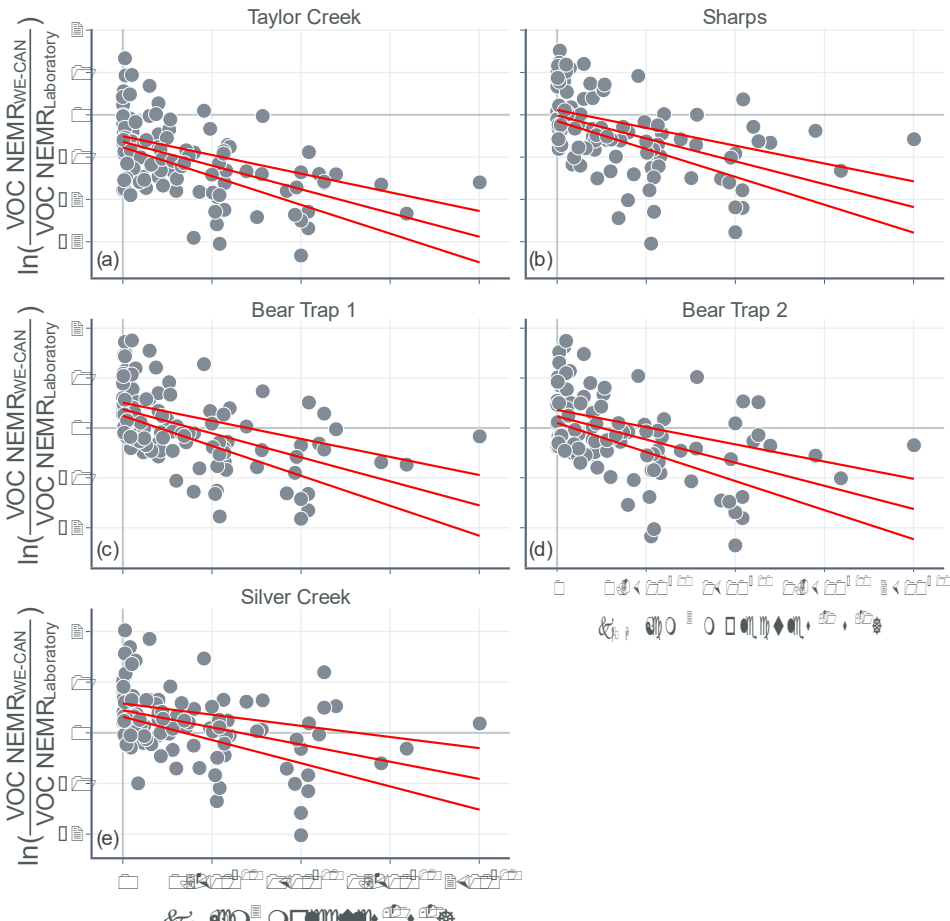


153 evolution of OA mass and O:C with time, and because all the required measurements were available to
154 perform the proposed OA modeling.

155 A suite of gas, particle, meteorological, and remote sensing instrumentation was deployed on the
156 NSF/NCAR C-130 to comprehensively characterize the smoke emissions and its environment. Below, we
157 briefly discuss the measurements and data products that relate to the scope of this work. Pressure and
158 temperature were measured using base instrumentation available onboard the aircraft.^{68,69} CO was
159 quantified using a Quantum-Cascade Tunable Infrared Laser Direct Absorption Spectrometer (QC-
160 TILDAS, Aerodyne Research) and reported at 1 Hz.⁷⁰ CO was assumed to be an inert tracer and used to
161 model dilution with the background air and to develop convenient metrics to characterize the OA
162 evolution with physical age. VOC mixing ratios were quantified using a Proton-Transfer-Reaction Time-
163 of-Flight Mass Spectrometer (PTR-ToF-MS 4000, Ionicon Analytik) at 1 Hz.³⁴ The PTR-ToF-MS
164 quantified concentrations for 122 VOCs, including the most important SOA precursors that have been
165 identified for biomass burning in previous work.^{37,38} A High-Resolution Aerosol Mass Spectrometer (HR-
166 AMS; Aerodyne Research) measured the mass concentrations and composition of the sub-micron, non-
167 refractory aerosol every 5 seconds.²⁰ Measurements of aerosol mass concentrations and OA elemental
168 ratios of H:C and O:C from the HR-AMS measurements were used here. A Single Particle Soot
169 Photometer (SP2; Droplet Measurement Technologies) quantified BC mass concentrations every 10
170 seconds.²⁰ Finally, aerosol size distributions were measured using a Passive Cavity Aerosol Spectrometer
171 Probe (PCASP) at 1 Hz⁷¹ and these were used to inform the shape of the initial aerosol size distribution
172 (median and geometric standard deviation). We used the 10 second merge data for all the measurements
173 mentioned above and conversions were performed when necessary to calculate concentrations at ambient
174 conditions (instead of at standard temperature and pressure conditions). Links to the data are provided in
175 the 'Data Availability' section.

176 We determined transect-average values for OA, non-OA
177 (sulfate+nitrate+ammonium+chloride+BC), CO, and VOC concentrations as well as the OA O:C and the
178 number size distributions. Following earlier published work with the WE-CAN data,^{20,33,68,69} we identified
179 the plume-sampling periods by visually examining the CO time series for increases and decreases in
180 mixing ratios. These averages were then corrected for background conditions by computing a universal
181 background value for each measured species (e.g., CO, OA, benzene) using all data from outside the
182 plume while the aircraft performed a transect set. This method assumed that the composition of the gas
183 and aerosol species in the background air remained constant in time and space. We also calculated a
184 normalized excess mixing ratio (NEMR) for OA and VOCs by ratioing its background-corrected
185 concentration (in $\mu\text{g m}^{-3}$ for OA and ppbv for VOCs) with the background-corrected CO (in ppbv). The
186 background-corrected OA O:C was calculated as a ratio of the background-corrected molar
187 concentrations for O and C; equations can also be found in Hodshire et al.⁷² For this calculation, we
188 assumed the OA to be only composed of C, H, and O such that the molar concentrations of C, H, and O
189 were determined from the available OA, O:C, and H:C data. While wildfire OA is likely to be composed
190 of nitrogen-containing organic compounds, the low N:C values measured during WE-CAN (~ 0.02)
191 (Garofalo et al., 2009) meant that accounting for nitrogen had a negligible impact on the reported OA
192 mass concentrations and O:C and H:C values. Background corrections were performed separately for
193 each wildfire plume transect set. We studied the sensitivity of the findings from this work to other ways in
194 which the background values can be calculated and these are described later (Section 3.2).
195





Wildfire	Taylor Creek	Sharps	Bear Trap 1	Bear Trap 2	Silver Creek
Physical Age [minutes]	21	45	53	56	32
OH Exposure [molecules cm ⁻³ hr]	$3.1 \times 10^6 \pm 0.7 \times 10^6$	$3.0 \times 10^6 \pm 0.7 \times 10^6$	$2.7 \times 10^6 \pm 0.7 \times 10^6$	$2.6 \times 10^6 \pm 0.7 \times 10^6$	$1.9 \times 10^6 \pm 0.7 \times 10^6$
Average OH Conc. [molecules cm ⁻³]	$8.9 \times 10^6 \pm 2.0 \times 10^6$	$4.0 \times 10^6 \pm 0.9 \times 10^6$	$3.0 \times 10^6 \pm 0.8 \times 10^6$	$2.8 \times 10^6 \pm 0.7 \times 10^6$	$3.5 \times 10^6 \pm 1.3 \times 10^6$
Intercept	-0.64 ± 0.1	-0.02 ± 0.1	0.02 ± 0.1	0.23 ± 0.1	0.45 ± 0.1
R-squared	0.26	0.23	0.26	0.21	0.16
RMSE	0.768	0.812	0.665	0.735	0.625

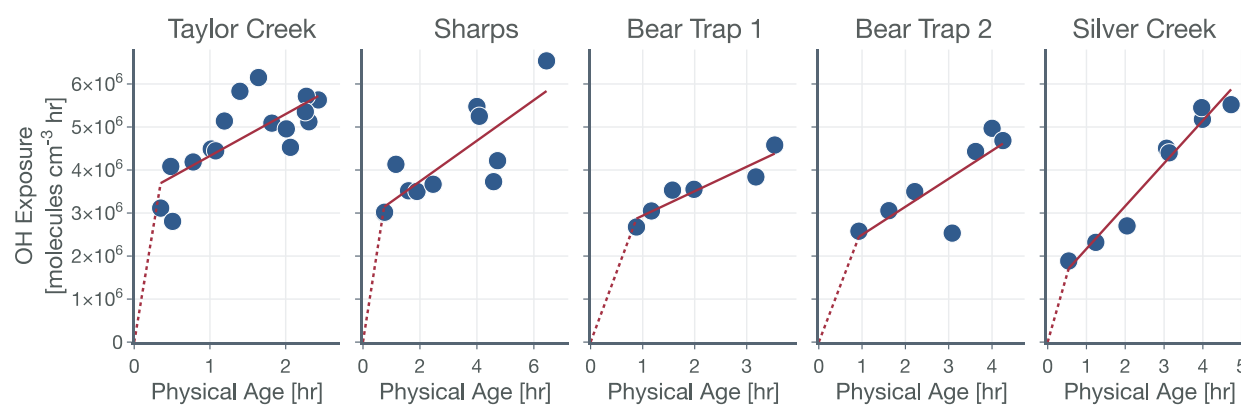
196
197 *Figure 1: Logarithm of the ratios of the VOC NEMR in the first transect of the wildfire plume to the*
198 *average value of the VOC NEMR measured in laboratory experiments plotted against k_{OH} . Results are*
199 *shown for the (a) Taylor Creek, (b) Sharps, (c) Bear Trap 1, (d) Bear Trap 2, and (e) Silver Creek Fire*
200 *transect sets. Solid red lines represent the linear fit to the data and the red bands capture the standard*
201 *error. The table lists statistics based on the linear fit including the OH concentration and exposure. The*
202 *time-varying OH exposures for all five transect sets are shown in Figure 2 and the OH concentrations are*
203 *listed again in Table 1.*

2.2 OH Concentration and Exposure Estimates

204 The hydroxyl radical (OH) exposure in the wildfire plumes was determined by examining the
205 laboratory-normalized and reactivity-differentiated VOC decay. For each transect in a wildfire plume, this
206 calculation was done by first taking the natural logarithm of the ratio of the VOC NEMRs at that transect
207 to the average values of the VOC NEMRs measured in laboratory experiments. The VOC NEMRs from
208 laboratory experiments were based on the work of Koss et al.²⁸ who measured emissions from 58 separate
209

211 burns performed on 18 different fuels. We decided to use the average values of the VOC NEMR across
 212 the 58 burns instead of using fuel-specific VOC NEMRs because the wildfire emissions sampled during
 213 WE-CAN arose from the combustion of a mixture of fuel types. Furthermore, we also did not consider
 214 differences in the burn conditions (e.g., differences in the modified combustion efficiency) between the
 215 laboratory experiments and wildfire plumes. As this calculation could only be performed when the
 216 corresponding VOC NEMRs were also available from the laboratory experiments, we performed this
 217 calculation on 106 out of the 122 VOCs measured by the PTR-ToF-MS. We assumed that the reactive
 218 oxygenated VOC concentrations in the wildfire plume were largely from direct emissions from the fire
 219 rather than produced through in-plume chemical reactions. This field-to-laboratory ratio of VOC NEMRs
 220 was then plotted against the reaction rate constant for those VOCs with OH (k_{OH}). The k_{OH} values for the
 221 VOCs are from those reported in Koss et al.²⁸ noting that they reflect k_{OH} values for either the most
 222 dominant isomer, weighted average of the potential isomers, or a VOC that is structurally similar. Here,
 223 we used k_{OH} values reported at 300 K to perform this analysis. As k_{OH} values for well-studied VOCs such
 224 as alkanes, alkenes, and aromatics are only $\pm 20\%$ off at the cooler temperatures in the wildfire plume
 225 compared to those at 300 K, accounting for the temperature-dependent k_{OH} is unlikely to change the OH
 226 estimates presented here. Isoprene, monoterpenes, and catechol can also react with O_3 in addition to OH
 227 and were excluded from the analysis, although including these VOCs did not appear to change the
 228 estimated OH exposure (not shown). This result was partly because the O_3 mixing ratios in the wildfire
 229 plume were low enough (45-90 ppbv) that these VOCs still preferentially reacted with OH rather than O_3 .
 230

231 Results for the first transect from the five transect sets analyzed in this work are shown in Figure
 232 1, as an example. The ratio of VOC NEMRs exhibited an inverse relationship with k_{OH} . The likely
 233 explanation for this inverse trend was that the oxidation chemistry prior to this transect resulted in
 234 stronger depletion of VOCs with a higher k_{OH} and weaker depletion of VOCs with a lower k_{OH} . An
 235 alternate explanation is that the ratio of VOC NEMRs was biased lower for the higher k_{OH} species
 236 compared to the lower k_{OH} species on account of differences in fuel and burn conditions as well as the
 237 timing of the emissions, but we are not aware of why there might be systematic changes in the emissions
 238 with the species k_{OH} . Assuming that chemistry prior to the first transect explains the trends in Figure 1, the
 239 slope in the ratio of VOC NEMRs with k_{OH} was fit to determine an effective OH exposure for the time
 240 period before this transect. We should note that we did not assume that the field and laboratory VOC
 241 NEMRs at the time of emission were the same, which would require setting the intercept for the fit to 0,
 242 which we did not do. Rather, we assumed that there were no systematic k_{OH} -dependent differences in
 243 emissions between the field and laboratory cases. This exercise was repeated for all transects to calculate
 244 a time-varying OH exposure estimate for all transect sets, results for which are shown in Figure 2. A line
 245 was fit through the OH exposure data to calculate an average OH concentration for the wildfire plume
 246 after the first transect. We assumed that the OH exposure changed linearly from zero, close to the fire, to
 247 the OH exposure estimated at the first transect, which resulted in a separate, time-invariant OH
 248 concentration estimate for the time period before the first transect.



249

250 **Figure 2: Time-varying OH exposures estimated for the five transects sets: (a) Taylor Creek, (b) Sharps,**
 251 **(c) Bear Trap 1, (d) Bear Trap 2, and (e) Silver Creek. The solid red lines are linear fits to time periods**
 252 **after the first transect while the dotted red lines represent the estimated OH exposure prior to the first**
 253 **transect. The lighter colored lines represent one standard deviation.**

254
 255 The OH concentrations before and after the first transect are tabulated for the five transect sets in
 256 Table 1. For the five transect sets and four fires analyzed, the total mean OH exposure varied between
 257 4.6×10^6 (Bear Trap 2) and 6.5×10^6 (Sharps) molecules-hr cm^{-3} to produce 1.7 to 4.4 hours of
 258 photochemical aging at an average OH concentration of 1.5×10^6 molecules cm^{-3} . The OH concentrations
 259 varied between 2.8×10^6 (Bear Trap 2) and 8.9×10^6 (Taylor Creek) before the first transect and between
 260 4.7×10^5 (Sharps) and 9.9×10^5 (Silver Creek) beyond the first transect. This analysis approach suggests
 261 that OH concentrations, on average, were a factor of six larger before the first transect compared to after
 262 the first transect suggesting that photochemical oxidation was as relevant to the wildfire plume in the near
 263 field (between the point of emission and the first transect) as it was for the far field (beyond the first
 264 transect) after accounting for differences in the physical age before and after the first transect; the first
 265 transect was estimated between 21 and 56 minutes of the physical age of the wildfire plume.

266 We assessed our estimates of OH concentrations in the wildfire plumes after the first transect and
 267 found them to be consistently lower than those estimated in previous work. For instance, our estimates for
 268 OH concentration in the Taylor Creek and Bear Trap wildfire plumes after the first transect (9.7×10^5 and
 269 $\sim 6 \times 10^6$ molecules cm^{-3} , respectively) were a factor of five to eight smaller than previous OH estimates for
 270 the same wildfire plumes calculated from the observed decay for a handful of VOCs in the core of the
 271 plume ($\sim 3 \times 10^6$ and $\sim 5 \times 10^6$ molecules cm^{-3} , respectively).⁶⁹ Similarly, our estimates of OH concentration
 272 after the first transect, across all five transect sets, were a factor of five to ten smaller than those estimated
 273 in Mexican and African biomass burning plumes^{44,48,53} where OH concentrations were calculated using
 274 techniques similar to those outlined in Juncosa Calahorrano et al.⁶⁹ We tentatively argue that the historical
 275 estimates of OH concentrations in wildfire plumes are larger and different than those measured here
 276 because earlier work has only used a few species (<5) to calculate OH concentrations. We hypothesize
 277 that our approach, which uses a much larger number of species (106), provides a more robust estimate for
 278 mean OH concentrations in the plume. However, this discrepancy in OH concentrations needs to be
 279 investigated in detail in future work. Finally, our estimated OH concentrations were found to be lower
 280 than the average OH concentrations typically found in urban environments and regional backgrounds
 281 ($\sim 1.5 \times 10^6$ molecules cm^{-3}).⁷³ In this specific urban and regional comparison, the low OH concentrations
 282 in the wildfire plume might be a result of the large OH sinks present therein as well as the low
 283 photochemical activity expected in optically dense plumes.⁷⁴

284
 285 **Table 1: Mean OH concentration and OH exposure estimates based on the ratio of VOC NEMRs for the**
 286 **five transect sets.**

Fire	OH Concentration (molecules cm^{-3})		OH Exposure (molecules-hr cm^{-3})	
	Before 1 st transect	After 1 st transect	At 1 st transect	At final transect
Taylor Creek	8.9×10^6	0.97×10^6	3.1×10^6	5.7×10^6
Sharps	4.0×10^6	0.47×10^6	3.0×10^6	6.5×10^6
Bear Trap 1	3.0×10^6	0.57×10^6	2.7×10^6	4.6×10^6
Bear Trap 2	2.8×10^6	0.65×10^6	2.6×10^6	4.7×10^6
Silver Creek	3.5×10^6	1.0×10^6	1.9×10^6	5.5×10^6

287 We note that the OH estimates used in this work are uncertain. The OH estimates are likely to be
 288 unbiased if the field and laboratory emissions ratios have no systematic relationship with k_{OH} . In case
 289 there is a relationship and that this relationship is different between the field and laboratory, our OH
 290 estimates could be biased lower or higher. Hence, there is no clear way in which we could argue that our
 291 OH estimates bound the range of expected values in a wildfire plume. Since the OH estimates were
 292

293 developed based on the observed decay of all species including reactive oxygenated VOCs, any chemical
294 production of oxygenated species should bias our OH estimate lower. Hence, based on the inclusion of
295 the reactive oxygenated VOCs alone, our OH estimates potentially present a lower bound estimate.
296 Although there is limited evidence, Coggon et al. (2019) have found in laboratory experiments performed
297 on biomass burning smoke that there was little to no production of reactive oxygenated VOCs, such as
298 phenol and furan, relative to these species' primary emissions. When OH was calculated from
299 hydrocarbon VOCs measured by the PTR-ToF-MS to eliminate the influence from including oxygenated
300 VOCs, the inverse relationship was weakened and produced OH concentrations that were at least a factor
301 of 2 lower than those listed in Table 1, both before and after the first transect. We also calculated OH
302 concentrations beyond the first transect by using the VOC NEMRs at the first transect as the reference
303 instead of using the VOC NEMRs from the laboratory. The concentrations so calculated and limited to
304 the time period beyond the first transect were found to be only slightly higher to those listed in Table 1
305 (0.67×10^6 - 1.2×10^6 molecules cm^{-3}) but still lower than those in historical studies mentioned earlier. The
306 VOC NEMRs at the first transect, by definition, cannot be used to determine the OH concentrations prior
307 to the first transect. Given the uncertainty, we studied the sensitivity of the findings from this work to the
308 OH concentrations before and after the first transect and these are described later (Section 3.2).
309

310 2.3 Organic Aerosol Model

311 We developed a plume version of the SOM-TOMAS model to simulate the formation,
312 composition, and evolution of OA in wildfire plumes. The statistical oxidation model (SOM), uses a
313 statistical approach to track the multigenerational oxidation chemistry and thermodynamic properties of
314 OA precursors and its oxidation products.^{75,76} The Two Moment Aerosol Sectional model (TOMAS),
315 uses a sectional approach to track the number and mass moments of the aerosol size distribution to
316 simulate the microphysical processes of nucleation, coagulation, and condensation/evaporation.^{77,78} The
317 SOM has been extensively used to study the influence of multi-generational aging,⁷⁹ IVOCs,⁸⁰ NO_x ,⁸¹ and
318 vapor wall losses in chambers^{65,82} on OA evolution. More recently, the SOM-TOMAS model was used to
319 study the SOA formation from biogenic VOCs,⁸³ phenols,⁸⁴ and evaporated petro- and bio-fuels.⁸⁵
320 Pertinent to this work, the SOM-TOMAS model was used to study the SOA formation in chamber
321 experiments performed on wildfire emissions.³⁸ The SOM-TOMAS model configuration described in
322 detail in Akherati et al.³⁸ was used in this work with modifications to account for dilution, different
323 environmental conditions (e.g., pressure, temperature) and an updated treatment of POA and SVOCs.
324

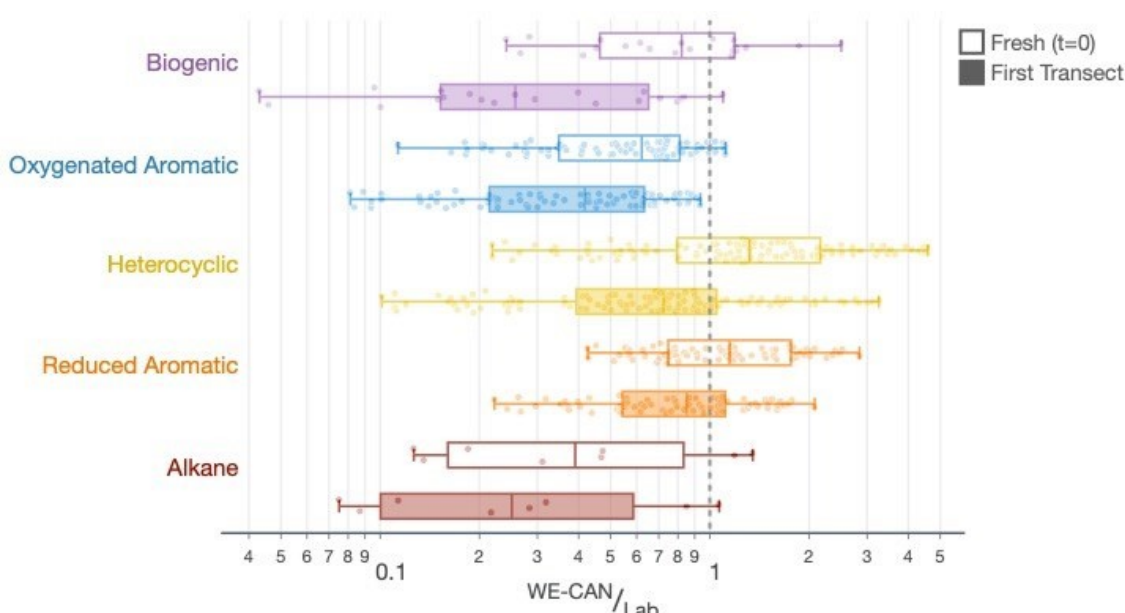
325 The SOM tracks the chemical evolution of OA and its precursors using a two-dimensional,
326 carbon (N_C) and oxygen (N_O) number grid. The properties of each model species (e.g. reactivity (k_{OH}),
327 volatility (c^*)) are parameterized based on their N_C and N_O . The SOM has six adjustable parameters that
328 govern the oxidation chemistry and thermodynamic properties of the model species: (i–iv) $p_{f,1}$ - $p_{f,4}$, the
329 yields of four functionalized products that add one, two, three, and four oxygen atoms to the carbon
330 backbone, respectively; (v) m_{frag} , the parameter that characterizes the fragmentation probability (P_{frag});
331 and (vi) ΔLVP , the decrease in the c^* of the model species per addition of an oxygen atom. The particle-
332 phase species in SOM are tracked in 36 TOMAS size sections that span dry diameters between 3 to
333 10,000 nm. TOMAS simulates coagulation between size sections and the kinetic
334 condensation/evaporation of mass between the particle and vapor phases for all SOM model species. The
335 SOM-TOMAS model also accounts for formation of highly oxygenated organic molecules (HOMs) and
336 formation/dissociation of oligomers.⁸³ The SOM-TOMAS model was also updated recently with the
337 diffusive-reactive framework described in Zaveri et al.⁸⁶ to model the influence of phase state on the
338 kinetic gas/particle partitioning of OA.⁸³ Although SOA precursors found in biomass burning emissions
339 (e.g., monoterpenes) are known to form HOMs (Ehn et al., 2014; Stolzenburg et al., 2018) and oligomers
340 (D'Ambro et al., 2018; Zaveri et al., 2020) and certain biomass burning particles can be viscous, neither
341 HOM nor oligomer formation was modeled and the OA was assumed to be liquid-like with a diffusion
342 coefficient of $10^{-10} \text{ m}^2 \text{ s}^{-1}$. These assumptions surrounding HOMs, oligomers, and phase state will need to
be examined in future work.



343 For each wildfire plume, the SOM-TOMAS model was used to simulate the OA evolution from
 344 the time just after emission up to the last measured transect. While this should include both vertical plume
 345 rise and horizontal plume transport after reaching the equilibrium height, we do not explicitly model the
 346 change in the pressure and temperature of the air parcel during vertical plume rise. The background-
 347 corrected CO concentrations past the first transect were first fit to an exponential function and the CO
 348 values including those extrapolated to $t=0$ were then used to determine dilution of the wildfire plume with
 349 background air starting at $t=0$. Since we only used background-corrected values in this work, we assumed
 350 the background air to be free of any trace gases and particles. This assumption affects non-linear
 351 processes, such as equilibrium partitioning and coagulation; however, because background concentrations
 352 are generally much lower than in-plume concentrations, these are expected to have a minimal effect.⁶³
 353 While the pressure and temperature values changed modestly between wildfire plumes, they were found
 354 to be in a relatively narrow range within each individual wildfire plume (Figure S2). Hence, an average
 355 pressure and temperature value was used for the entire wildfire plume. Model predictions and
 356 measurements of concentrations and mixing ratios in this work were expressed at the plume pressure and
 357 temperature.
 358

359 **2.4 SOA Formation from VOCs**

360 SOA formation from VOCs was modeled similarly to the treatment presented in Akherati et al.³⁸
 361 Briefly, we considered five broad classes of SOA precursors, with the surrogates informing the SOA
 362 formation listed in parentheses: (i) alkanes (*n*-dodecane; Loza et al.⁸⁷), (ii) aromatic hydrocarbons
 363 (benzene, toluene, *m*-xylene; Ng et al.⁸⁸ and Zhang et al.⁶⁵), (iii) oxygenated aromatics (phenol, guaiacol,
 364 syringol; Yee et al.⁸⁹), (iv) heterocyclics (2-methylfuran+dimethylfuran; He et al.⁸⁵), and (v) biogenics
 365 (isoprene, α -pinene; Chhabra et al.⁹⁰). We did not model the SOA formation from partially speciated
 366 VOCs as we did not find them to be important SOA precursors in our previous work.³⁸ Akherati et al.³⁸
 367 found that the five organic classes mentioned above, on average, were able to explain most of the SOA
 368 measured in chamber experiments performed on emissions from laboratory fires, with oxygenated
 369 aromatics and heterocyclic compounds accounting for 80% of the SOA produced. The SOM-TOMAS
 370 parameters, specific to high NO_x conditions, to model SOA formation from these precursors are listed in
 371 Table S1. Each of the 67 SOA precursors in the model were assigned an SOA surrogate, mentioned in
 372 parentheses above, and this surrogate assignment along with the molecular weight and k_{OH} value for the
 373 precursor is listed in Table S2. We also modeled SOA formation from SVOCs and that treatment is
 374 described in Section 2.5.
 375



377 *Figure 3: Ratio of VOC NEMRs at t=0 and the first transect in the wildfire plume to the average values of*
 378 *VOC NEMRs measured in laboratory experiments. Data are aggregated by the following SOA precursor*
 379 *class: biogenics, oxygenated aromatics, heterocyclics, aromatic hydrocarbons, and alkanes. Within each*
 380 *SOA precursor class, data are presented together for all five transect sets such that each point represents*
 381 *the ratio for a given VOC NEMR in a specific transect.*

382
 383 The VOC NEMRs at the first transect were extended to t=0 by correcting for the OH exposure
 384 before the first transect (see Table 1 for transect-set-specific OH exposures). These field VOC NEMRs at
 385 t=0 and the first transect were aggregated by precursor class and compared to the VOC NEMRs measured
 386 by Koss et al.²⁸ during a recent laboratory campaign. Results of this comparison, combined over all five
 387 transect sets and four wildfires, are shown in Figure 3. Results when separated by transect set were
 388 similar to those presented in Figure 3 and, hence, are not shown or discussed. The VOC NEMRs for the
 389 five SOA precursor classes at the first transect were substantially lower than those measured in the
 390 laboratory. The median values at the first transect were 74%, 58%, 28%, 15%, and 75% lower for the
 391 biogenic, oxygenated aromatic, heterocyclic, aromatic hydrocarbons, and alkane classes, respectively,
 392 compared to the laboratory values. The largest differences were observed for the most reactive SOA
 393 precursors with respect to OH (e.g., oxygenated aromatics) and the smallest differences were observed for
 394 the least reactive SOA precursors with respect to OH (e.g., aromatic hydrocarbons), a feature that was
 395 leveraged to determine the OH concentrations and exposure in Section 2.2. Even after correcting for OH
 396 exposure prior to the first transect, the VOC NEMRs for three of the organic classes (i.e., biogenic,
 397 oxygenated aromatic, and alkane) were still modestly lower compared to those measured in the
 398 laboratory. The median values at t=0 were 18%, 38%, and 61% lower for the biogenic, oxygenated
 399 aromatic, and alkane classes, respectively, compared to the laboratory values. The median values were
 400 32% and 15% higher for the heterocyclic and aromatic hydrocarbon classes, respectively, compared to the
 401 laboratory values.

402 There are two important implications of the differences in the ratios of VOC NEMRs shown in
 403 Figure 3 and described in the previous paragraph. First, field emissions of SOA precursors (those at t=0)
 404 are lower than those measured in laboratory experiments, for at least a few of the important organic
 405 classes. It is expected then that the SOA precursor mixture would be relatively less potent in forming
 406 SOA in wildfire plumes than what has been observed in laboratory experiments.^{37-39,41-43} Second, a
 407 significant fraction of the SOA precursor emissions are depleted between t=0 and the first transect
 408 (between 15% and 74%). This implies that not only is SOA being actively produced in the near field after
 409 emission (<1 hour) but also that there is significantly reduced potential for continued production of SOA
 410 beyond the first transect. These comparisons partly explain the field versus laboratory differences outlined
 411 by Hodshire et al.,⁴⁰ for the OA evolution after the first transect.

413 **2.5 Treatment of POA and SVOCs**

414 POA was treated as semivolatile and reactive, following a history of observations from laboratory
 415 experiments.^{21,22,91} Fresh emissions of POA close to the fire were determined in an iterative manner.
 416 Using an initial guess for the POA mass concentration at t=0, we fit a mass distribution for eight model
 417 species in the SOM grid that was able to reproduce the average volatility behavior observed by May et al.
 418²² for POA emissions (Figure S3a). May et al.²² measured this average volatility behavior by studying the
 419 response of fresh POA emissions from 19 separate fires and 12 different fuels to dilution and thermal
 420 denuding in laboratory experiments. The model species were placed in a SOM grid for multi-ring
 421 aromatics ($\Delta LVP=1.4922$), the reason for which is discussed later in this section. The number of model
 422 species (i.e., 8) used to represent the POA and SVOC mass in the SOM grid was arbitrary and the use of a
 423 larger number of model species (e.g., 10, 15) did not seem to affect our results (not discussed further).
 424 The following species were used to represent the POA/SVOC mass in the SOM grid: C₅O₇, C₉O₂, C₉O₅,
 425 C₁₁O₂, C₁₂O₂, C₁₂O₃, C₁₄O₅, and C₁₅O₆ (Figure S3c). An explanation for why this precise set of species
 426 was used is presented later when describing results from the sensitivity (Monte-Carlo) simulations
 427 (Section 3.2). In addition to constraining the mass distribution in the SOM grid to match observations of

428 POA volatility, the model species were deliberately chosen to produce a specific response in the aerosol
429 O:C with POA mass concentration, following observations of biomass burning OA in laboratory²¹ and
430 field⁹² environments (Figure S3b): an increasing OA O:C from with a decrease in OA mass concentration
431 from 1000 to 1 $\mu\text{g m}^{-3}$. The SOM-TOMAS model was used to simulate the time period between t=0 and
432 the first transect using the POA value assumed at t=0, and this process was iterated until the OA mass
433 concentration at the first transect was the same as the measured value. This method necessarily assumes
434 that the OA mass and composition at t=0 is different from that at the first transect. As the assumptions
435 about POA volatility and oxidation chemistry were altered across different simulations, this iterative
436 approach to determining the POA mass concentration at t=0 was done separately for each simulation and
437 transect set.

438 We used the detailed speciation data for POA and SVOCs from Jen et al.²⁵ to create a substitute
439 volatility distribution, which was then used to study the sensitivity in model results to the volatility
440 distribution assumed for POA and SVOCs. Jen et al.²⁵ used two-dimensional gas chromatography with
441 time-of-flight mass spectrometry (GC \times GC-ToF-MS) on derivatized samples to measure the detailed
442 chemical composition of POA and SVOC emissions from 29 laboratory-generated fires performed on 24
443 different fuels. They measured ~150 unique species in the sample collected on quartz filters and these
444 amounted to between 10 and 65% of the total POA/SVOC mass. The averaged and normalized volatility
445 distribution and mass distribution in carbon-oxygen space for the POA and SVOC emissions is shown in
446 Figures S4a and S4b, respectively. The volatility distribution was constructed by binning the ~150 species
447 by c^* , which was estimated for each species using EPISuite 4.11,⁹³ a numerical model that estimates
448 physical and chemical properties of pure substances.

449 Jen et al.²⁵ found that the SVOC emissions were dominated by sugars, phenols, and other
450 complex organic compounds (e.g., terpenoids, heterocyclics), organic compound classes also measured by
451 the PTR-ToF-MS. In theory, there should be little if any overlap between the SOA precursors quantified
452 by the PTR-ToF-MS and GC \times GC-ToF-MS since the PTR-ToF-MS exclusively sampled gas-phase
453 compounds with a c^* higher than $10^5 \mu\text{g m}^{-3}$ ²⁸ and the GC \times GC-ToF-MS measurement was performed on
454 quartz filters that generally trap gas- and particle-phase compounds lower than a c^* of $10^5 \mu\text{g m}^{-3}$.²² In this
455 work, we assumed that the SVOCs and VOCs represent a mutually exclusive set of SOA precursors
456 despite similarities in the compound classes within these two categories. SVOCs have been hypothesized
457 to be important precursors of SOA formation from biomass burning emissions,^{20,33} but there are few
458 laboratory datasets that can be called upon to inform the oxidation chemistry of SVOCs in our model. In
459 addition to Jen et al.,²⁵ several studies have measured semivolatile multi-ring aromatics in biomass
460 burning emissions and they are expected to serve as SOA precursors.^{23,35,94} Hence, in the absence of any
461 model SOA precursors for which laboratory data are available, we simulated the oxidation chemistry of
462 SVOCs in the base configuration of the SOM-TOMAS model assuming that they have a similar potential
463 to form SOA as multi-ring aromatics (i.e., naphthalene). However, given the uncertainty in this
464 assumption, we performed sensitivity simulations where we modeled the oxidation chemistry of SVOCs
465 as oxygenated aromatics (i.e., phenol), heterocyclics (i.e., 2-methylfuran+dimethylfuran), linear alkanes
466 (i.e., *n*-dodecane), or biogenics (i.e., α -pinene) with the species in parentheses used as the surrogate to
467 model SOA formation (Section 3.2).

468 2.6 Model Configuration and Simulations

469 The base simulations were performed with the following model configuration. We assumed POA
470 to be semivolatile and reactive. The representation of POA/SVOC mass in the SOM grid was based on
471 the volatility distribution of May et al.²² and the oxidation chemistry for SVOCs was modeled based on
472 SOM parameters for multi-ring aromatics (naphthalene). We assumed a liquid-like phase state to model
473 the kinetics of OA gas/particle partitioning. All SOA parameters, including those for SVOCs and VOCs,
474 were corrected for the influence of vapor losses to the walls of the Teflon chamber. Background
475 corrections were performed on the raw observations using a background value that was specific to each
476 wildfire transect set, but not varying in time or space for that transect set. The OH concentrations were
477 based on an analysis of the ratios of VOC NEMRs, with separate but constant values for the time periods
478



479 before and after the first transect. The first transect for each transect set was hand chosen based on the
 480 transect closest to the fire that had the highest observed VOC NEMR. Simulations performed with this
 481 base model configuration are also referred to as the 'SV-POA+FullChem' simulations, representative of
 482 the most updated treatment of OA and OA precursors in wildfire plumes. Nearly all of the assumptions in
 483 the base model were rigorously tested by performing sensitivity simulations, as described below:

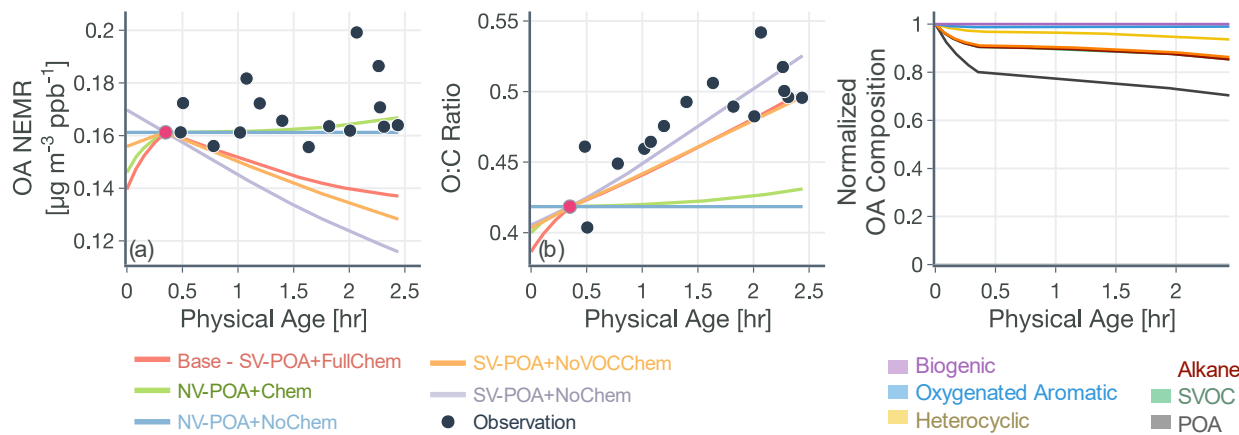
- 484 1. In addition to the base simulations (SV-POA+FullChem), we performed a systematic sequence of
 485 simulations where we tested assumptions about POA volatility and SVOC and VOC chemistry:
 486 (i) non-volatile POA and no chemistry (NV-POA+NoChem), (ii) non-volatile POA and VOC
 487 chemistry (NV-POA+Chem), (iii) semivolatile POA and no chemistry (SV-POA+NoChem), and
 488 (iv) semivolatile POA and SVOC chemistry (SV-POA+NoVOCChem). Results from these
 489 simulations are presented in Figures 4 and 5.
- 490 2. Simulations were performed to assess the sensitivity in model results to the treatment of POA and
 491 SVOCs: (i) we simulated the oxidation chemistry for SVOCs using the SOM parameters for
 492 oxygenated aromatics (i.e., phenol), heterocyclics (i.e., 2-methylfuran+dimethylfuran), linear
 493 alkanes (i.e., *n*-dodecane), or biogenics (i.e., α -pinene), with the species in parentheses used as
 494 the surrogate to model SOA formation, (ii) we used the POA volatility distribution determined
 495 from the work of Jen et al.²⁵ in combination with the five surrogate species to model the oxidation
 496 chemistry of SVOCs, and (iii) we performed a thousand Monte-Carlo simulations where we
 497 randomly chose eight species in the SOM grid to represent the POA and SVOC mass and fit a
 498 mass distribution with these eight species that reproduced the POA volatility behavior observed
 499 by May et al.²² Results from these simulations are presented in Figures 6 and S9-S10.
- 500 3. Simulations were performed to assess the sensitivity in model results to the assumed OH
 501 concentrations, 'first' transect, and background correction: (i) we assumed a low or high OH
 502 concentration over the entire wildfire plume with the low value based on the OH estimate after
 503 the first transect and the high value based on the OH estimate before the first transect (Table 1),
 504 (ii) we assumed a time-varying OH concentration that was determined by fitting a power function
 505 through the OH exposure data presented in Figure 2, (iii) we assumed a constant OH
 506 concentration of 1.5×10^6 molecules cm⁻³ that is commonly used to reflect average OH
 507 concentrations in polluted environments, (iv) instead of using the transect closest to the fire as the
 508 first transect, we assumed the second or third closest transects to be the 'first' transect to perform
 509 the simulations, and (v) measurements and model inputs were calculated by performing
 510 background corrections by using the transect-specific background concentrations or assuming the
 511 concentrations upwind of the fire to be representative of the true background. Results from these
 512 simulations are presented in Figures 7 and S11-S12.

514 3. Results

515 3.1 OA Mass and Composition Evolution

516 Results from simulations performed with the base configuration and with assumptions about POA
 517 volatility and oxidation chemistry are shown in Figure 4 for the Taylor Creek Fire. We present results for
 518 Taylor Creek first because the sampling strategy was the most Lagrangian in our dataset (Figure S1).
 519 Model predictions and measurements of OA mass are presented using the NEMR metric (Figure 4a) and
 520 those for OA composition as the background-corrected OA O:C (Figure 4b). Model predictions and
 521 measurements of the background-corrected OA and CO concentrations at ambient volume are shown in
 522 Figure S5. The measurements show mildly increasing OA NEMR ($0.16 \mu\text{g m}^{-3}$ ppbv⁻¹) with an increase in
 523 the OA O:C (from ~ 0.41 to ~ 0.52) and these trends were used to evaluate predictions from the five
 524 different model simulations. Uncertainties in the observed OA NEMR and O:C were deliberately left out
 525 since those were found to be much larger than the overall trend, which made it harder to evaluate the
 526 model predictions. A version of Figure 4 that includes the standard error in the mean for the observed OA
 527 NEMR and O:C is presented as Figure S6.





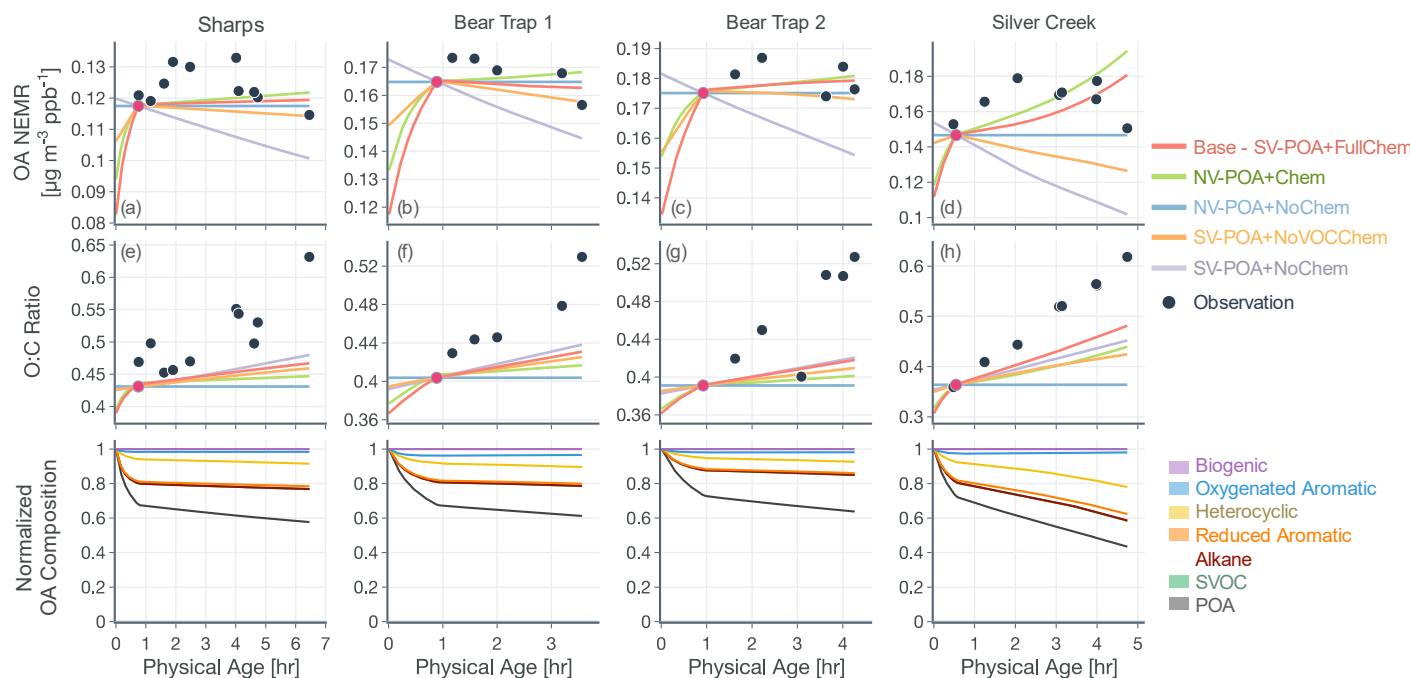
529
530 *Figure 4: Predictions of (a) OA NEMR and (b) OA O:C from the SOM-TOMAS model (solid colored*
531 *lines) compared against measurements (solid black circles) from the Taylor Creek Fire. Model*
532 *predictions are shown for five different simulations that vary in their assumptions about POA volatility*
533 *and SVOC and VOC oxidation chemistry. Model predictions were always constrained to the*
534 *measurements of OA NEMR and OA O:C at the 1st transect, marked by the red solid circle. Predictions of*
535 *the normalized OA composition from the base simulations are shown in panel (c).*

536
537 For the simulations with non-volatile POA and no oxidation chemistry (NV-POA+NoChem), the
538 model reproduced observations of OA NEMR (Mean Bias Error (MBE)=−0.009, Mean Absolute Error
539 (MAE)=0.011; $\mu\text{g m}^{-3}$ ppbv $^{-1}$) but, by definition, produced no change in the OA O:C (MBE=−0.060,
540 MAE=0.062). With the oxidation chemistry turned on to produce SOA from VOCs (NV-POA+Chem),
541 the model only produced a marginal increase in the OA NEMR compared to the NV-POA+NoChem
542 simulation and, hence, reproduced observations of OA NEMR (MBE=−0.007, MAE=0.011; $\mu\text{g m}^{-3}$ ppbv $^{-1}$).
543 The NV-POA+Chem simulation produced a slight increase in OA O:C with physical age compared to
544 the NV-POA+NoChem model but still significantly lower than the observed increase in OA O:C (MBE=−
545 0.055, MAE=0.057). The relatively small increase in OA NEMR and OA O:C can be explained by the
546 marginal amounts of SOA formed from the VOC mixture beyond the first transect. As noted in Section
547 2.4, this VOC mixture was substantially depleted in important SOA precursors by the first transect. For
548 the simulation with semivolatile POA with no oxidation chemistry (SV-POA+NoChem) and the
549 simulation with semivolatile POA with oxidation chemistry for SVOCs alone (SV-POA+NoVOCChem),
550 the model appeared to underestimate the OA NEMR (MBE=−0.035 and -0.028, MAE=0.035 and 0.028,
551 respectively; $\mu\text{g m}^{-3}$ ppbv $^{-1}$) with a substantial increase in OA O:C. The predicted decrease in OA NEMR
552 compared to the NV-POA+NoChem model stemmed from the evaporation of POA with dilution that was
553 only partly recovered through SOA formation in the SV-POA+NoVOCChem model. Results from the
554 SV-POA+NoChem simulation suggested that POA evaporation alone could explain the increase in the
555 OA O:C with physical age as the lower-volatility material left in the particle phase after evaporation had a
556 relatively higher O:C than the semivolatile material that had evaporated (Figure S3b).

557 The base simulation that assumed a semivolatile POA and oxidation chemistry for both SVOCs
558 and VOCs (SV-POA+FullChem) underestimated the OA NEMR by 15% compared to observations
559 (MBE=−0.024, MAE=0.024; $\mu\text{g m}^{-3}$ ppbv $^{-1}$) but produced a large increase in OA O:C consistent with the
560 observations (MBE=−0.019, MAE=0.032; $\mu\text{g m}^{-3}$ ppbv $^{-1}$). The base simulation predicted a lower increase
561 in O:C compared to the SV-POA+NoChem simulation because the SOA being formed in the base
562 simulation had a lower O:C than the remaining POA. Overall, two of the simulations appeared to be the
563 most consistent with observations of OA NEMR but significantly underestimated the observations of OA
564 O:C (NV-POA+NoChem and NV-POA+Chem), and two of the simulations came close to reproducing
565 the increase in OA O:C with physical age but underestimated the observations of OA NEMR (SV-
566 POA+NoChem and SV-POA+NoVOCChem). The base or SV-POA+FullChem simulation seemed to

567 offer a balanced comparison with observations where both the OA NEMR and O:C were only slightly
568 underestimated.

569 Results from simulations for the remaining fires and transect sets (Sharps, Bear Trap, and Silver
570 Creek) are shown in Figure 5(a-h), where the relative trends across the five different simulations were
571 similar to those presented for Taylor Creek in Figure 4. Therefore, the differences in these simulations are
572 not described further. However, as discussed below, the absolute performance of the base simulation for
573 these other transect sets was mixed. The base simulation could not reproduce the initial increase and later
574 decrease in observed OA NEMR for the Sharps and Silver Creek Fires. Both of these fires were sampled
575 by the aircraft much faster than the physical age (Figure S1), suggesting that the measurements may
576 reflect changes in emissions rather than those from their physicochemical evolution. The base simulation
577 produced a mildly increasing OA NEMR for the Sharps Fire (MBE=-0.004, MAE=0.006; $\mu\text{g m}^{-3}$ ppbv⁻¹)
578 and a sharply increasing OA NEMR for the Silver Creek Fire (MBE=-0.004, MAE=0.012; $\mu\text{g m}^{-3}$ ppbv⁻¹).
579 Unlike the comparison for the Taylor Creek Fire, the base simulation appeared to reproduce the relatively
580 constant observations of OA NEMR for the Bear Trap Fire transects. The base simulations produced a
581 different trend in the modeled OA NEMR with physical age across the five different transect sets because
582 presumably, in each of these transect sets, there were differences in the dilution rate, environmental
583 conditions, and absolute concentrations of the OA, OA precursors, and oxidants. The base simulation
584 consistently underestimated the change in OA O:C with physical age, with the strongest comparison for
585 the Bear Trap 1 Fire (MBE=-0.044, MAE=0.044) and the weakest comparison for the Silver Creek Fire
586 (MBE=-0.087, MAE=0.087).
587



588
589 *Figure 5: Predictions of (a-d) OA NEMR and (e-h) OA O:C from the SOM-TOMAS model compared
590 against measurements (solid black circles) from four different wildfire transect sets (Sharps, Bear
591 Trap x 2, Silver Creek). Model predictions are shown for five different simulations that vary in their
592 assumptions about POA volatility and oxidation chemistry. (i-l) Model predictions of the normalized OA
593 composition from the base simulations (SV-POA+FullChem).*

594 Taken together, we draw the following conclusions from the model-measurement comparisons
595 presented in Figures 4 and 5. First, a non-volatile and non-reactive treatment of POA, regardless of the
596 inclusion of SOA produced from VOC oxidation, is unlikely to explain the combined observations of OA
597 NEMR and O:C. Second, POA evaporation with dilution alone can potentially explain the change in the
598

599 OA O:C with time but results in loss of OA mass (decrease in OA NEMR) that is not consistent with
600 observations. Third, we argue that POA evaporation with dilution with SOA formation from both SVOCs
601 and VOCs, as captured by the base model, best explains the trends in both the OA NEMR and OA O:C
602 across the five transect sets and four wildfires: average MBE=-0.007 and MAE=0.011 ($\mu\text{g m}^{-3}$ ppbv $^{-1}$) for
603 OA NEMR and average MBE=-0.046 and MAE=0.055 for OA O:C across all five transect sets. We note
604 that the model treatment in the base simulations closely reflects our updated understanding of the POA
605 and SOA system from wildfire emissions.

606 Model predictions of the normalized OA composition with physical age from the base
607 simulations are shown in Figure 4c for the Taylor Creek Fire and in Figures 5(i-l) for all other transect
608 sets while model predictions of the POA-SOA split with photochemical age for all transect sets are shown
609 in Figure S7. There are several interesting features to note. The OA composition began to change rapidly
610 starting at t=0 from the dilution-driven evaporation of directly emitted POA and the SOA produced from
611 the oxidation of SVOCs and VOCs. By the first transect, the average OA across all five transect sets, 21
612 to 56 minutes after emission, was 73% POA and 27% SOA. As the base-simulation-predicted OA NEMR
613 was found to universally increase during the period before the first transect for all five transect sets, the
614 changes in OA composition were largely driven by SOA condensation rather than POA evaporation. The
615 rapid SOA production was facilitated by the higher OH concentrations experienced before the first
616 transect ($2.9\text{--}8.9 \times 10^6$ molecules cm^{-3} ; see Table 1). Generally speaking, the observed and base-
617 simulation-predicted OA NEMRs did not vary much past the first transect for any of the transect sets.
618 Despite that fact, the base simulations predicted a modest change in the OA composition with physical
619 age after the first transect, suggesting a roughly equal replacement of POA with SOA. Over all five
620 transect sets, POA continued to dominate the total OA mass beyond the first transect (>45%) but there
621 was continued production of SOA over this time period. By the last transect, the SOA contribution to the
622 total OA varied between 30% for the Taylor Creek Fire and 56% for the Silver Creek Fire.

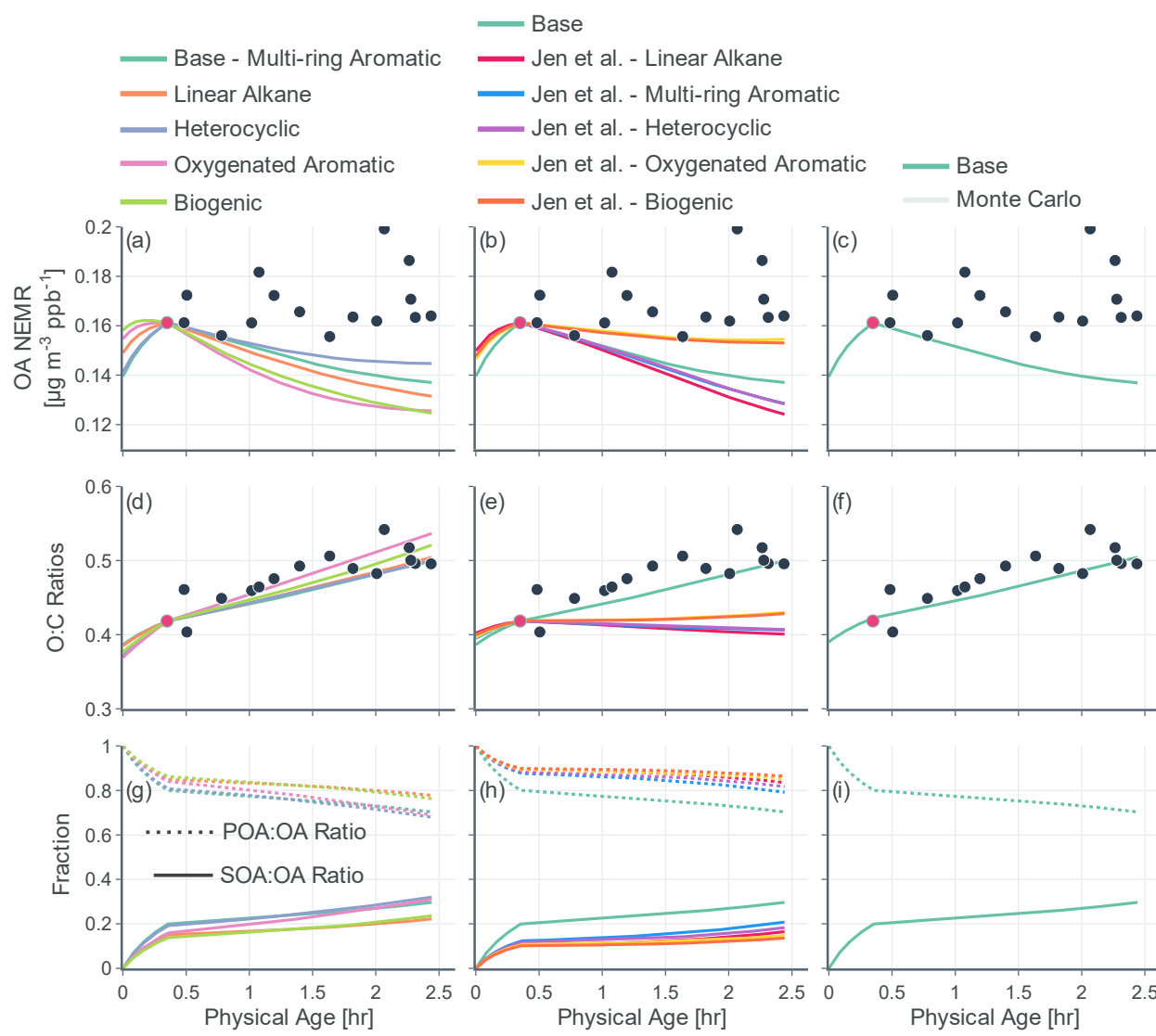
623 The base simulations predicted that the majority of the SOA was formed from the oxidation of
624 SVOCs, heterocyclics, and oxygenated aromatics, in that order. The contribution of the different VOC
625 classes to SOA formation was similar between the different transect sets, although oxygenated aromatics
626 contributed much more to SOA formation in the Silver Creek Fire than in the other Fires. On average,
627 these three precursor classes accounted for 45, 25, and 21% of total SOA and 18, 11, and 9% of the total
628 OA by the last transect. Heterocyclics and oxygenated aromatics have already been implicated as
629 important SOA precursors in laboratory experiments performed on biomass burning emissions^{37–39,95} and
630 our results here confirm their relevance for wildfire plumes as well. Biogenic VOCs were found to be
631 significantly less influential compared to the precursor classes just discussed where they accounted for
632 less than 5% of total SOA and 2% of total OA by the last transect.

633 These simulations provide model-based evidence for dilution-driven evaporation of POA mass
634 being replaced by SOA mass formed from the oxidation of SVOCs and VOCs in wildfire plumes during
635 WE-CAN. This conclusion is consistent with the theoretical findings of Bian et al.⁶² and Hodshire et al.,⁶³
636 who showed that POA evaporation can be approximately replaced with SOA condensation under certain
637 conditions pertaining to the fire size, background concentrations, and atmospheric stability. The base
638 simulations predicted a mean POA-SOA split of 59%-41% by the last transect over all five transect sets.
639 These model-predicted POA-SOA splits agreed well with the theoretical findings of Hodshire et al.,⁶³
640 who predicted a POA-SOA split of ~50-50% for 1 km^2 fires and ~75-25% for 100 km^2 fires, and the
641 findings of Palm et al.,³³ who analytically determined a maximum POA-SOA split of 66%-33% for OA
642 measured over several wildfire plumes during WE-CAN. Note that Palm et al.³³ estimated their maximum
643 POA-SOA split assuming that the OA at the first transect was exclusively POA. In contrast to the
644 precursor-resolved findings discussed above, Palm et al.³³ proposed that SVOCs were responsible for
645 nearly 90% of the SOA formed within the plume. However, their approach would overestimate the SVOC
646 contribution to SOA because the underlying closure calculation subtracted the SOA estimated from non-
647 SVOC precursors from the total SOA formed.

649 3.2 Sensitivity in Model Predictions



650 Results from simulations performed to assess the sensitivity to the model treatment of POA and
 651 SVOCs are shown in Figure 6. Here, we compare model predictions of OA NEMR (top row) and OA O:C
 652 (middle row) against measurements for the Taylor Creek Fire and plot model predictions of the fractional
 653 contributions of POA and SOA to OA (bottom row). We also include predictions from the base
 654 simulation shown in Figure 4. Results from sensitivity simulations performed for the other transect sets
 655 are shown in Figures S9-10. In the base simulation, SVOCs accounted for <20% of the total OA by the
 656 last transect. Despite the relatively small contribution of SVOCs to total OA, the use of different surrogate
 657 species to simulate the oxidation chemistry of SVOCs resulted in a moderate spread in the OA NEMR
 658 predictions, with all predictions biased lower than the measurements. The use of a heterocyclic surrogate
 659 (i.e., 2-methylfuran+dimethylfuran) seemed to agree the best, and the use of an oxygenated aromatic
 660 surrogate (i.e., phenol) seemed to agree the least with the OA NEMR observations. The differences in the
 661 model predictions were understandable since the potential to form SOA is known to vary substantially
 662 across the five surrogate species considered: naphthalene, *n*-dodecane, 2-methylfuran+dimethylfuran,
 663 phenol/guaiaacol, and α -pinene. There was a similar spread in the model predictions of OA O:C but, in
 664 contrast to the OA NEMR comparisons, all model predictions compared reasonably with the observed
 665 increase in the OA O:C. The spread in the model predictions of OA O:C was between 0.5 and 0.53 at the
 666 last transect. The average OA split was 75% POA and 25% SOA by the last transect.
 667



668

669 *Figure 6: Predictions of (a,b,c) OA NEMR and (d,e,f) OA O:C from the SOM-TOMAS model (solid*
670 *colored lines) compared against measurements (solid black circles) from the Taylor Creek Fire. (g,h,i)*
671 *Predictions of the fractional contributions of POA and SOA to OA. Model predictions are shown for*
672 *sensitivity simulations performed with varying assumptions for the (a,d,g) SVOC oxidation chemistry,*
673 *(b,e,h) POA volatility and SVOC oxidation chemistry, and (c,f,i) POA+SVOC mass distribution in the*
674 *SOM grid (Monte-Carlo).*

675
676 On using the substitute volatility distribution based on the speciation data of Jen et al.,²⁵ the
677 model produced a relatively larger spread in the OA NEMR predictions compared to the sensitivity result
678 discussed above. The use of an oxygenated aromatic (i.e., phenol/guaiacol) and biogenic (i.e., α -pinene)
679 surrogate seemed to agree the best and the use of a heterocyclic (i.e., 2-methylfuran+dimethylfuran),
680 multi-ring aromatic (i.e., naphthalene), and linear alkane (i.e., *n*-dodecane) surrogate seemed to agree the
681 least with the OA NEMR observations. All simulations produced a flat response in the OA O:C with
682 physical age despite a gradual change in the POA-SOA split and dilution-driven evaporation of the
683 semivolatile material. This flat response, which was inconsistent with the observed change in the OA
684 O:C, was primarily from the lower-volatility material that was left in the particle phase being less
685 oxidized than the higher volatility material that had evaporated (Figure S4c). The substitute volatility
686 distribution resulted in a larger POA-SOA split (average of 83%-17%) compared to the first set of
687 sensitivity results (average of 75%-25%) likely because a smaller fraction of the fresh POA mass was lost
688 to evaporation from the use of a less volatile volatility distribution (Figures S4a and S4d). The mixed
689 comparisons for OA NEMR and O:C suggest that model inputs determined from speciation data hold
690 promise but might be limited because, in this specific case, the speciated compounds only represented a
691 fraction (10-65%) of the total POA+SVOC mass.

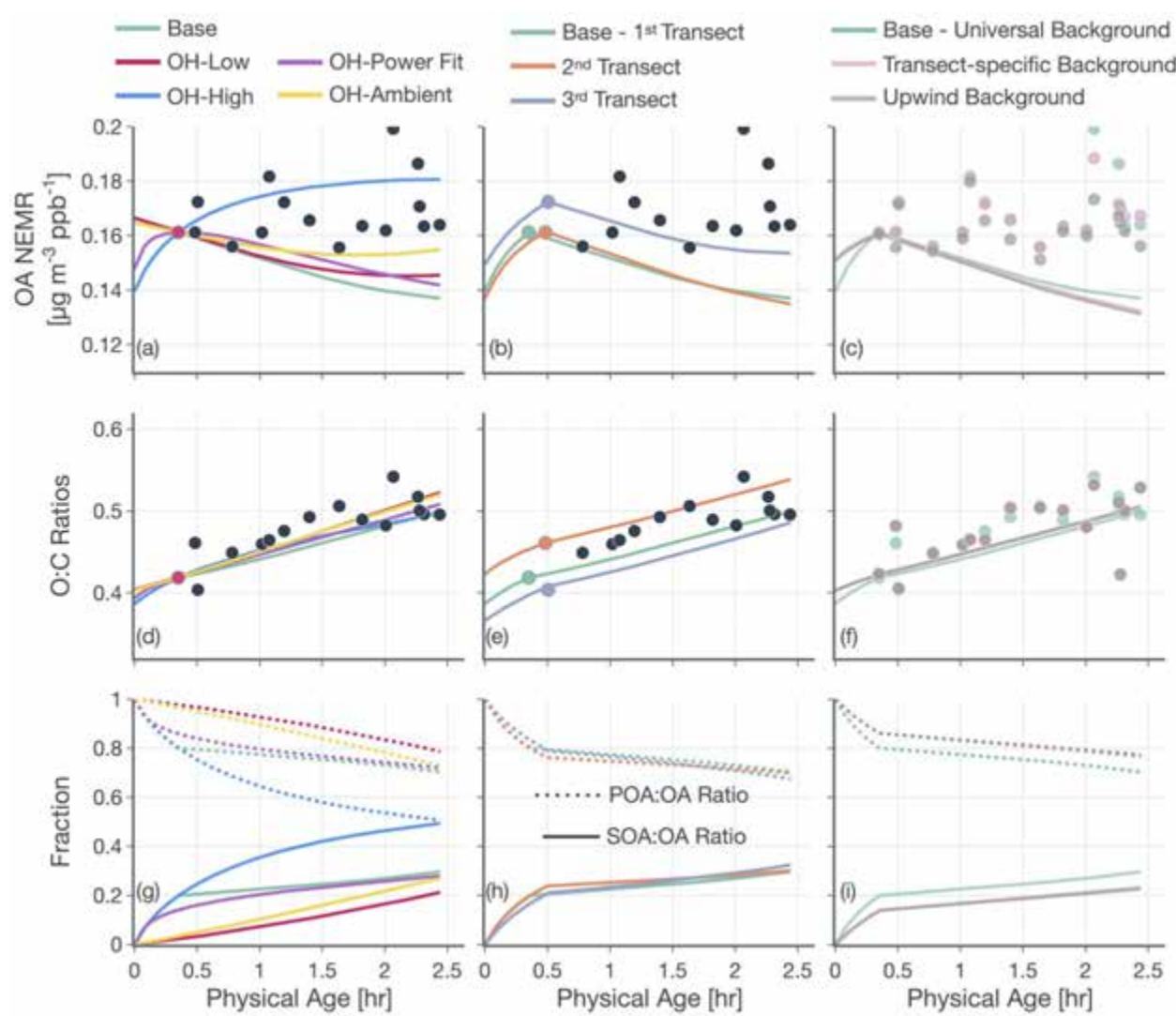
692 Finally, we performed a thousand Monte-Carlo simulations where we randomly specified the
693 mass distribution of the POA+SVOC mass in the SOM grid while ensuring that this mass distribution
694 reproduced the POA volatility behavior observed by May et al.²² (Figure S8). The iterations produced a
695 relatively narrower spread in the OA NEMR predictions compared to the previous sensitivity simulations
696 but they all seemed to underestimate the observed trends. By the last transect, the predicted OA NEMR
697 was 17 to 29% lower than the average observed OA NEMR. Compared to the OA NEMR, there was a
698 much larger spread in the predicted OA O:C with iterations predicting a decrease in O:C with physical
699 age at the one end (from 0.41 to 0.31) to reproducing the observed increase at the other end (0.38 to 0.54).
700 It appears that the mass distribution of POA+SVOC in the SOM grid had a significant, non-linear
701 influence on POA evaporation, SOA production, and subsequently on the OA O:C evolution with
702 photochemical age. We note that the mass distribution of POA+SVOC in the SOM grid across the
703 thousand simulations was always constrained to observations of POA volatility but had enough degrees of
704 freedom to produce a substantial spread in model predictions. The iteration that resulted in the largest
705 absolute OA NEMR at the end of the simulation and then the largest increase in OA O:C was chosen to
706 represent the base simulation results presented in Figures 4 and 5. In other words, the distribution of
707 POA+SVOC mass in the SOM grid for the base simulation was chosen from amongst those used in the
708 Monte-Carlo simulations that produced the most optimum comparison against measurements of OA
709 NEMR and O:C for the Taylor Creek Fire. There is some indirect evidence for this POA+SVOC mass
710 distribution in that the O:C dependence with OA mass loading seemed to agree qualitatively with a subset
711 of laboratory and field observations of biomass burning OA^{21,92} (not shown).

712 Results from simulations performed to assess the sensitivity to the OH estimates are presented in
713 Figure 7(a,d,g). The use of a power function fitted to the OH exposure data to determine OH
714 concentrations (OH-Power Fit) produced results that were slightly higher compared to those from the base
715 simulation. Similarly, if we assumed that the lower OH concentration after the first transect was also
716 relevant to the time period before the first transect (OH-Low; 9.7×10^5 molecules cm⁻³), the model
717 predictions of OA NEMR and O:C were slightly higher than those from the base simulation. When using
718 a constant OH concentration of 1.5×10^6 molecules cm⁻³ (OH-Ambient) or the higher OH concentration
719 from before the first transect (OH-High; 8.9×10^6 molecules cm⁻³) for the entire evolution, the model



720 predicted a higher OA NEMR compared to predictions from the base, OH-Power Fit, and OH-Low
 721 simulations. This was because the OH concentrations after the first transect in both of these instances
 722 were larger than those used in the base, OH-Power Fit, and OH-low simulations and these higher OH
 723 concentrations, which were ~50% larger in OH-Ambient and a factor of ~10 larger in OH-High, promoted
 724 SOA formation.

725 For the OH-High simulation, the increase in OA NEMR was found to be relatively consistent
 726 with the evolution in the observations indicating that the OH concentrations may continue to be elevated
 727 even after the first transect. However, the OH-High simulations overestimated the OA NEMR compared
 728 to the observations for the other Fires (Figure S11), where the base, OH-Power Fit, and OH-Low
 729 simulations produced results that were more in line with the observations. As the Taylor Creek Fire
 730 dataset is the most Lagrangian amongst all Fires, the OH sensitivity simulation results presented here
 731 provide some evidence that our OH concentration estimates after the first transect (Table 1) may be
 732 biased low and would need to be revised in future work to be consistent with the higher OH
 733 concentrations estimated in earlier work (see Section 2.2 for a longer discussion). Interestingly, a higher
 734 OA NEMR in the OH-High simulation did not change predictions for OA O:C presumably because the
 735 additional SOA formed had an O:C similar to the existing OA's O:C. Overall, the model predictions
 736 appeared to be somewhat sensitive to the OH concentration inputs that produced a significant spread in
 737 the OA NEMR and POA-SOA splits but not so much in the OA O:C.
 738



739

740 *Figure 7: Predictions of (a,b,c) OA NEMR and (d,e,f) OA O:C from the SOM-TOMAS model (solid*
741 *colored lines) compared against measurements (solid black circles) from the Taylor Creek Fire. (g,h,i)*
742 *Predictions of the fractional contributions of POA and SOA to OA. Model predictions are shown for*
743 *sensitivity simulations performed with varying assumptions for OH (a,d,g), reference transect (b,e,h), and*
744 *approach to performing background corrections.*

745 Qualitatively, the modeled trends in the OA NEMR and OA O:C were not very different when we
746 assigned different transect sets (i.e., ‘2nd Transect’, ‘3rd Transect’) to be the ‘1st transect’ where model
747 predictions of OA NEMR and OA O:C were anchored to observations; results are presented in Figure
748 7(b,e,h). There appeared to be some tradeoff in the model-measurement comparisons for OA NEMR and
749 OA O:C with the transect chosen. For instance, anchoring the model predictions to the information at the
750 third transect seemed to produce better agreement with observations of OA NEMR but underestimated
751 observations of OA O:C. The opposite was found to be true when anchoring the model predictions to the
752 information at the second transect. Regardless of the variability in the OA NEMR and O:C, the POA-
753 SOA splits were nearly identical between the three simulations. The use of ‘Transect-Specific’ or
754 ‘Upwind’ data to calculate values to perform the background corrections did not seem to have any
755 significant effect on model predictions; results are presented in Figure 7(c,f,i).

756 **4. Implications of the Base Simulation Results**

757 A summary of the model predictions from the base simulations for POA, SOA, and the SOA
758 precursor NEMRs at t=0 and the first and last transects, for all five transect sets is presented in Figure 8.
759 Some of these results have been presented in Figures 4 and 5 earlier but this specific presentation of the
760 results provides an opportunity to summarize the modeling effort and draw broader implications.

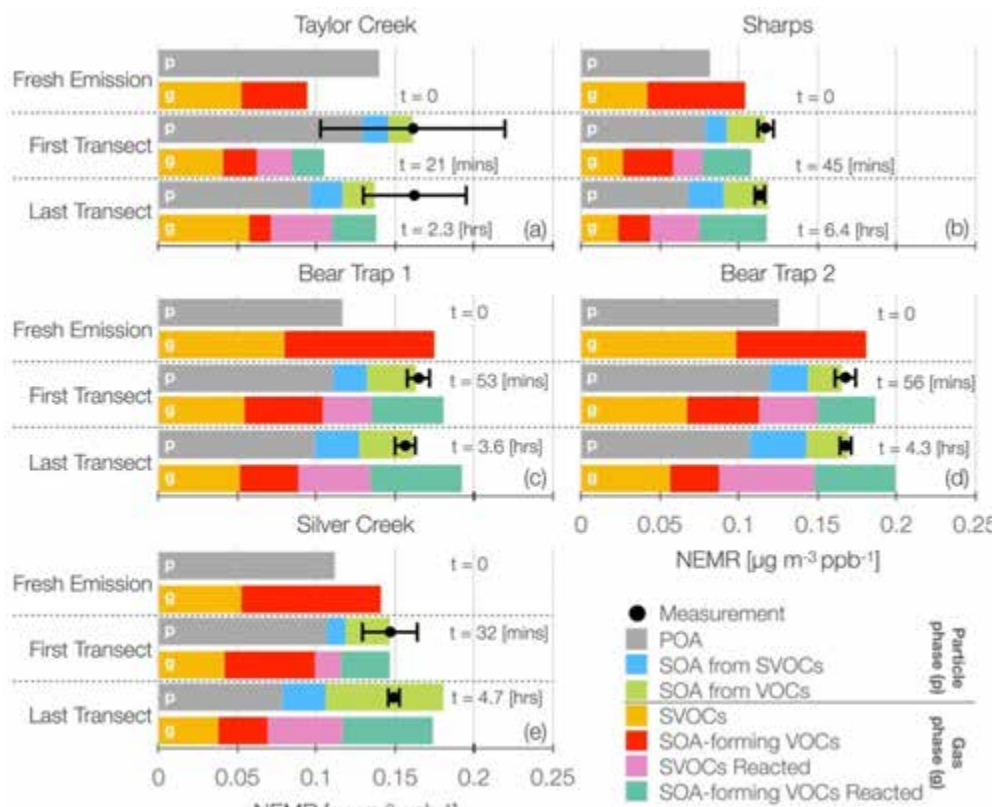
761 First, fresh emissions of POA were found to be similar in magnitude to the sum of SOA-forming
762 SVOCs and VOCs. For reference, for mobile sources, SOA precursor emissions are easily an order of
763 magnitude larger than those for POA.^{29,96} This means that direct emissions of POA are likely to be an
764 important constituent of smoke aerosol downwind of the fire, even as some fraction of it is lost to
765 evaporation and surface reactions (not modeled in this work) and SVOCs and VOCs oxidize to form SOA
766 and add to OA mass.

767

768

769





770
771 *Figure 8: Model predictions of OA and SOA precursor NEMRs at t=0 ('Fresh Emission') and the first*
772 *and last transects for all five transect sets. Observations of OA NEMR are also presented for the first*
773 *and last transects in black with error bars.*

774
775 Second, up to half of the SOA precursor mass was rapidly oxidized to form SOA early on, which
776 primarily resulted in an increase in the OA NEMR and O:C prior to the first transect. This result implies
777 that a substantial fraction of the total SOA is actually formed very close to the fire and that the OA
778 measured on the first aircraft transect is likely to be enhanced compared to the fresh OA emissions
779 measured in laboratory experiments, after accounting for differences in gas/particle partitioning at
780 different OA mass loadings. Furthermore, the rapid evolution of the OA system close to the fire is bound
781 to alter the chemical, microphysical, and optical properties of smoke aerosols early on and confound
782 comparisons of aerosol measurements at the first transect with similar measurements made on fresh
783 emissions in laboratory environments.

784 Third, for most of the modeled and measured transect sets, except for the model prediction for the
785 Silver Creek Fire, the OA NEMR did not vary much between the first and last transects, but there was a
786 gradual change in the modeled OA composition with POA evaporation and SOA formation from SVOCs
787 and VOCs. This is consistent with both theoretical and analytical findings in Bian et al.,⁶² Hodshire et
788 al.,⁶³ Palm et al.,³³ and Liang et al.⁶⁷ The change in composition implies that while the OA mass may
789 remain constant, its atmospheric properties will continue to evolve with physical age. Furthermore, as the
790 SOA precursors were heavily depleted and the OA mass concentrations at the last transect (5-30 $\mu\text{g m}^{-3}$)
791 were only marginally larger than the background concentrations (1-20 $\mu\text{g m}^{-3}$), we postulate that the OA
792 NEMR and O:C are unlikely to change dramatically with additional photochemical aging, any different
793 than the changes experienced by background aerosol.

794 Fourth, by the last transect, SVOCs and VOCs contributed about equally to SOA formation in our
795 wildfire plumes. The dominant SVOCs and VOCs contributing to SOA formation are very likely to be
796 oxygenated organic compounds (e.g., sugars, heterocyclics, oxygenated aromatics), classes that are not

797 explicitly included or are represented too coarsely in emissions inventories and chemical mechanisms,
798 part of atmospheric models. Hence, the representation of SOA formation, as studied here, needs to be
799 reflected for biomass burning sources in atmospheric models.
800

801 5. Conclusions, Uncertainties, and Directions for Future Work

802 In this study, we used a plume version of a kinetic model to simulate the dilution and
803 physicochemical evolution of OA in wildfire plumes measured during the WE-CAN field campaign. The
804 model was built on parameterizations developed from laboratory data, initialized using field
805 measurements, and evaluated against the OA mass and composition measurements gathered from pseudo-
806 Lagrangian transect sets. Our work suggests that it is very likely that dilution-driven evaporation of
807 semivolatile POA and simultaneous photochemical production of SOA from SVOCs and VOCs explain
808 the relative invariability in OA enhancements with photochemical age in observations of ambient wildfire
809 plumes. These findings around OA evolution are consistent with the theoretical analyses presented by
810 Bian et al.⁶² and Hodshire et al.⁶³ as well as the analytical findings of Palm et al.³³ and Liang et al.⁶⁷ In
811 addition, our model predictions indicate an important role for oxidation chemistry and rapid SOA
812 formation before the first aircraft measurements, which is likely to be driven by higher-than-ambient OH
813 concentrations in the wildfire plume (3×10^6 to 10^7 molecules cm⁻³). Notionally, for the fires studied here,
814 we expect the OA measured within an hour after emission to be 80% POA and 20% SOA and 60% POA
815 and 40% SOA after several additional hours of evolution. SOA precursor emissions for a few important
816 organic classes (i.e., oxygenated aromatics, biogenics) appear to be systematically lower than those
817 measured in laboratory experiments, and these lower emissions might partly explain the reduced
818 propensity to form SOA in wildfire plumes. Finally, oxygenated compound classes such as sugars,
819 heterocyclics, and oxygenated aromatics within SVOCs and VOCs are likely to serve as important
820 precursors for SOA formation in wildfire plumes.

821 Model results were found to be moderately sensitive to the treatment for POA and SVOCs.
822 Hence, continued work to fully speciate the POA and SVOC mass to inform the volatility properties of
823 POA and to identify surrogate species to model the oxidation chemistry of SVOCs will likely lead to
824 improvements in model predictions. A point of contention for SVOCs is that they have not been explicitly
825 considered when studying the SOA formation from biomass burning emissions in laboratory
826 experiments.^{37,38} Akherati et al.³⁸ observed that lower-volatility SOA precursors, especially in the SVOC
827 range, were susceptible to loss in transfer ducts used to direct smoke emissions into environmental
828 chambers. If this is indeed true, this might be one reason why SVOCs remain highly relevant for wildfire
829 plumes but may not have been for laboratory experiments. Regardless, the chemical composition and
830 oxidation chemistry of SVOCs relevant to SOA formation needs to be studied in the future.

831 We acknowledged a significant discrepancy in OH concentrations in the wildfire plume based on
832 techniques used in this work and OH concentrations estimated in earlier work. In addition, model
833 predictions were found to be somewhat sensitive to the OH concentrations assumed in the wildfire plume.
834 Hence, ongoing and future work needs to focus on developing and applying analytical and modeling
835 techniques to better estimate and evaluate OH concentrations in wildfire plumes. For instance, recently,
836 Peng et al.⁷⁴ calculated HO_x (OH + HO₂) production rates in wildfire plumes sampled during WE-CAN
837 from the photolysis of nitrous acid (HONO), O₃, and other smaller aldehydes (e.g., formaldehyde) and
838 ozonolysis of alkenes. These HO_x production rates could be used to inform OH concentrations. Similarly,
839 OH concentrations could be constrained by applying explicit gas-phase chemical mechanisms to
840 reproduce the time-dependent evolution of VOCs and their oxidation products in wildfire plumes.

841 In addition to the uncertainties alluded to in this work, there are several additional aspects to
842 consider while modeling the OA evolution in wildfire plumes. First, the model parameterizations in this
843 work (e.g., POA volatility, SOA parameters) were based on simpler model systems studied in laboratory
844 environments and these parameters may not accurately represent the processes in real wildfire plumes.
845 Most obviously, differences in the fuel complex, burn conditions, combustion efficiency, and
846 environmental conditions (e.g., temperature, relative humidity) and regimes (e.g., photolytic rates, NO_x)
847 could produce differences in the emissions, chemistry, and properties of OA and OA precursors between



848 the laboratory and the field.^{34,68} A more specific example is that the parameters that we used to model the
 849 SOA formation from SVOCs, heterocyclics, and oxygenated aromatics (precursor classes that contributed
 850 the most to SOA production) came from environmental chamber experiments performed on a handful of
 851 surrogate species (phenol, guaiacol, and syringol, 2-methylfuran+dimethylfuran, and naphthalene,
 852 respectively) under relatively dry (relative humidity<20%) and high NO_x conditions (200-800
 853 ppbv).^{85,89,97} While this extrapolation is typical for how laboratory data are translated into parameters for
 854 use in atmospheric models, these laboratory versus field differences need to be considered when
 855 evaluating model predictions against measurements.

856 Second, the physicochemical evolution modeled prior to the first transect remains extremely
 857 uncertain as there are no observations to evaluate those model predictions. Aircraft campaigns in the
 858 future should aim to characterize the near-field evolution in the hour after emission by performing
 859 transects closer to the fire when conditions allow. Moreover, campaigns should also accommodate
 860 repeated sampling of the near-field to assess changes in emissions over the same timescales used to
 861 perform the transect set. Any emissions changes would then need to be considered in interpreting the
 862 plume evolution inferred from the transect dataset.

863 Third, the current version of the SOM-TOMAS model does not simulate the photolysis or
 864 aqueous chemistry of OA or OA precursors. Photolysis has been shown to be an important loss pathway
 865 for SOA formed from monoterpenes.^{98,99} Oxygenated aromatics that include phenols, methoxyphenols,
 866 and phenolic carbonyls, after uptake into aerosol water, can participate in aqueous reactions to form low-
 867 volatility and light absorbing SOA.^{26,100} Both of these chemical processes are likely occurring in wildfire
 868 plumes and, hence, need to be included in future modeling efforts.

869 Fourth, the model initialization and evaluation in this work only relied on a subset of
 870 measurements made during WE-CAN. Future work could certainly benefit from leveraging an extended
 871 set of measurements gathered during WE-CAN and similar field campaigns focused on studying biomass
 872 burning emissions (e.g., BBOP¹⁰¹, LASIC¹⁰², FIREX-AQ (<https://csl.noaa.gov/projects/firex-aq/>)). For
 873 example, model predictions could be compared against measurements of the evolving composition (e.g.,
 874 oligomers), size distribution, and thermodynamic (e.g., volatility), optical (e.g., scattering, extinction),
 875 and climate (e.g., cloud condensation nuclei) properties.

876 Fifth, Peng et al.⁷⁴ and Hodshire et al.⁷² were recently able to study the distinct evolution of trace
 877 species resolved over the width of the wildfire plume. Both found evidence for increased photochemical
 878 activity near the edges and wings of the plume since these regions diluted much faster and were less
 879 optically dense compared to the core of the plume. Modeling in the future could use the information
 880 inherent in gradients within the transect to constrain the OA evolution under varying dilution and
 881 photochemical conditions.

882 And finally, the modeling in this work focused on simulating the plume evolution in a subset of
 883 large, daytime fires in the western US. In the future, the model will need to be applied to study a diversity
 884 of fires in terms of size, fuels, and geography (e.g., agricultural fires in the southeast US) to assess the
 885 broader applicability of the findings presented in this work.

886 5. Data Availability

887 Field campaign data from WE-CAN can be found at the permanent archival link:
 888 https://data.eol.ucar.edu/master_lists/generated/we-can/. The latest version of the SOM-TOMAS plume
 889 model along with the simulation data will be archived with Colorado State University Libraries when this
 890 paper is accepted for publication.

891 6. Author Contributions

892 AA, ALH, JRP, and SHJ designed the study. AA and YH developed the model and AA
 893 performed the simulations and analyzed the data. LAG, DKF, SMK, WP, LH, EVF, CNJ, AHG, TLC, FF,
 894 JMR, and DWT facilitated access to the field data and its appropriate use in the model. AA, JRP, and SHJ
 895 wrote the paper with contributions from all co-authors.



899 **7. Acknowledgements**

900 This work was supported by the National Oceanic and Atmospheric Administration
901 (NA17OAR4310003, NA17OAR4310001, NA17OAR4310010) and the U.S. Department of Energy
902 (DOE), Office of Science (DE-SC0017975). The WE-CAN field campaign was supported by the National
903 Science Foundation through grants AGS-1650786 and AGS-1650275.

904 **905 8. References**

906 (1) Andreae, M. O.; Merlet, P. Emission of Trace Gases and Aerosols from Biomass Burning. *Global*
907 *Biogeochem. Cycles* **2001**, *15* (4), 955–966 DOI: 10.1029/2000GB001382.

908 (2) Reid, J. S.; Koppmann, R.; Eck, T. F.; Eleuterio, D. P. A Review of Biomass Burning Emissions Part
909 II: Intensive Physical Properties of Biomass Burning Particles. *Atmos. Chem. Phys.* **2005**, *5* (3),
910 799–825 DOI: 10.5194/acp-5-799-2005.

911 (3) van der Werf, G. R.; Randerson, J. T.; Giglio, L.; Collatz, G. J.; Mu, M.; Kasibhatla, P. S.; Morton,
912 D. C.; DeFries, R. S.; Jin, Y.; van Leeuwen, T. T. Global Fire Emissions and the Contribution of
913 Deforestation, Savanna, Forest, Agricultural, and Peat Fires (1997–2009). *Atmos. Chem. Phys.* **2010**,
914 *10* (23), 11707–11735 DOI: 10.5194/acp-10-11707-2010.

915 (4) Akagi, S. K.; Yokelson, R. J.; Wiedinmyer, C.; Alvarado, M. J.; Reid, J. S.; Karl, T.; Crounse, J. D.;
916 Wennberg, P. O. Emission Factors for Open and Domestic Biomass Burning for Use in Atmospheric
917 Models. *Atmos. Chem. Phys.* **2011**, *11* (9), 4039–4072 DOI: 10.5194/acp-11-4039-2011.

918 (5) Yokelson, R. J.; Burling, I. R.; Gilman, J. B.; Warneke, C.; Stockwell, C. E.; de Gouw, J.; Akagi, S.
919 K.; Urbanski, S. P.; Veres, P.; Roberts, J. M.; Kuster, W. C.; Reardon, J.; Griffith, D. W. T.;
920 Johnson, T. J.; Hosseini, S.; Miller, J. W.; Cocker, D. R., III; Jung, H.; Weise, D. R. Coupling Field
921 and Laboratory Measurements to Estimate the Emission Factors of Identified and Unidentified Trace
922 Gases for Prescribed Fires. *Atmos. Chem. Phys.* **2013**, *13* (1), 89–116 DOI: 10.5194/acp-13-89-2013.

923 (6) Andreae, M. O. Emission of Trace Gases and Aerosols from Biomass Burning – an Updated
924 Assessment. *Atmos. Chem. Phys.* **2019**, *19* (13), 8523–8546 DOI: 10.5194/acp-19-8523-2019.

925 (7) Jimenez, J. L.; Canagaratna, M. R.; Donahue, N. M.; Prevot, A. S. H.; Zhang, Q.; Kroll, J. H.;
926 DeCarlo, P. F.; Allan, J. D.; Coe, H.; Ng, N. L.; Aiken, A. C.; Docherty, K. S.; Ulbrich, I. M.;
927 Grieshop, A. P.; Robinson, A. L.; Duplissy, J.; Smith, J. D.; Wilson, K. R.; Lanz, V. A.; Hueglin, C.;
928 Sun, Y. L.; Tian, J.; Laaksonen, A.; Raatikainen, T.; Rautiainen, J.; Vaattovaara, P.; Ehn, M.;
929 Kulmala, M.; Tomlinson, J. M.; Collins, D. R.; Cubison, M. J.; Dunlea, E. J.; Huffman, J. A.;
930 Onasch, T. B.; Alfarra, M. R.; Williams, P. I.; Bower, K.; Kondo, Y.; Schneider, J.; Drewnick, F.;
931 Borrmann, S.; Weimer, S.; Demerjian, K.; Salcedo, D.; Cottrell, L.; Griffin, R.; Takami, A.;
932 Miyoshi, T.; Hatakeyama, S.; Shimono, A.; Sun, J. Y.; Zhang, Y. M.; Dzepina, K.; Kimmel, J. R.;
933 Sueper, D.; Jayne, J. T.; Herndon, S. C.; Trimborn, A. M.; Williams, L. R.; Wood, E. C.;
934 Middlebrook, A. M.; Kolb, C. E.; Baltensperger, U.; Worsnop, D. R. Evolution of Organic Aerosols
935 in the Atmosphere. *Science* **2009**, *326* (5959), 1525–1529 DOI: 10.1126/science.1180353.

936 (8) Schill, G. P.; Froyd, K. D.; Bian, H.; Kupc, A.; Williamson, C.; Brock, C. A.; Ray, E.; Hornbrook,
937 R. S.; Hills, A. J.; Apel, E. C.; Chin, M.; Colarco, P. R.; Murphy, D. M. Widespread Biomass
938 Burning Smoke throughout the Remote Troposphere. *Nat. Geosci.* **2020**, *13* (6), 422–427 DOI:
939 10.1038/s41561-020-0586-1.

940 (9) Ramnarine, E.; Kodros, J. K.; Hodshire, A. L.; Lonsdale, C. R.; Alvarado, M. J.; Pierce, J. R. Effects
941 of near-Source Coagulation of Biomass Burning Aerosols on Global Predictions of Aerosol Size
942 Distributions and Implications for Aerosol Radiative Effects. *Atmos. Chem. Phys.* **2019**, *19* (9),
943 6561–6577 DOI: 10.5194/acp-19-6561-2019.

944 (10) Hobbs, P. V.; Reid, J. S.; Kotchenruther, R. A.; Ferek, R. J.; Weiss, R. Direct Radiative Forcing by
945 Smoke from Biomass Burning. *Science* **1997**, *275* (5307), 1776–1778 DOI:
946 10.1126/science.275.5307.1777.

947 (11) Yue, X.; Mickley, L. J.; Logan, J. A.; Kaplan, J. O. Ensemble Projections of Wildfire Activity and
948 Carbonaceous Aerosol Concentrations over the Western United States in the Mid-21st Century.
949 *Atmos. Environ.* **2013**, *77*, 767–780 DOI: 10.1016/j.atmosenv.2013.06.003.



Open Access Article. Published on 15 June 2022. Downloaded on 7/2/2022 12:56:50 AM.
This article is licensed under a Creative Commons Attribution-NonCommercial 3.0 Unported Licence.

(cc) BY-NC

950 (12) O'Dell, K.; Ford, B.; Fischer, E. V.; Pierce, J. R. Contribution of Wildland-Fire Smoke to US PM_{2.5}
951 and Its Influence on Recent Trends. *Environ. Sci. Technol.* **2019**, *53* (4), 1797–1804 DOI:
952 10.1021/acs.est.8b05430.

953 (13) McClure, C. D.; Jaffe, D. A. US Particulate Matter Air Quality Improves except in Wildfire-Prone
954 Areas. *Proc. Natl. Acad. Sci. U. S. A.* **2018**, *115* (31), 7901–7906 DOI: 10.1073/pnas.1804353115.

955 (14) Ford, B.; Val Martin, M.; Zelasky, S. E.; Fischer, E. V.; Anenberg, S. C.; Heald, C. L.; Pierce, J. R.
956 Future Fire Impacts on Smoke Concentrations, Visibility, and Health in the Contiguous United
957 States. *GeoHealth* **2018**, *2* (8), 229–247 DOI: 10.1029/2018GH000144.

958 (15) Chen, J.; Li, C.; Ristovski, Z.; Milic, A.; Gu, Y.; Islam, M. S.; Wang, S.; Hao, J.; Zhang, H.; He, C.;
959 Guo, H.; Fu, H.; Miljevic, B.; Morawska, L.; Thai, P.; Lam, Y. F.; Pereira, G.; Ding, A.; Huang, X.;
960 Dumka, U. C. A Review of Biomass Burning: Emissions and Impacts on Air Quality, Health and
961 Climate in China. *Sci. Total Environ.* **2017**, *579*, 1000–1034 DOI: 10.1016/j.scitotenv.2016.11.025.

962 (16) Spracklen, D. V.; Mickley, L. J.; Logan, J. A.; Hudman, R. C.; Yevich, R.; Flannigan, M. D.;
963 Westerling, A. L. Impacts of Climate Change from 2000 to 2050 on Wildfire Activity and
964 Carbonaceous Aerosol Concentrations in the Western United States. *J. Geophys. Res.* **2009**, *114*
965 (D20) DOI: 10.1029/2008jd010966.

966 (17) Carter, T. S.; Heald, C. L.; Jimenez, J. L.; Campuzano-Jost, P.; Kondo, Y.; Moteki, N.; Schwarz, J.
967 P.; Wiedinmyer, C.; Darmenov, A. S.; da Silva, A. M.; Kaiser, J. W. How Emissions Uncertainty
968 Influences the Distribution and Radiative Impacts of Smoke from Fires in North America. *Atmos.*
969 *Chem. Phys.* **2020**, *20* (4), 2073–2097 DOI: 10.5194/acp-20-2073-2020.

970 (18) Shrivastava, M.; Cappa, C. D.; Fan, J.; Goldstein, A. H.; Guenther, A. B.; Jimenez, J. L.; Kuang, C.;
971 Laskin, A.; Martin, S. T.; Ng, N. L.; Petaja, T.; Pierce, J. R.; Rasch, P. J.; Roldin, P.; Seinfeld, J. H.;
972 Shilling, J.; Smith, J. N.; Thornton, J. A.; Volkamer, R.; Wang, J.; Worsnop, D. R.; Zaveri, R. A.;
973 Zelenyuk, A.; Zhang, Q. Recent Advances in Understanding Secondary Organic Aerosol:
974 Implications for Global Climate Forcing: Advances in Secondary Organic Aerosol. *Rev. Geophys.*
975 **2017**, *55* (2), 509–559 DOI: 10.1002/2016RG000540.

976 (19) Lewis, K. A.; Arnott, W. P.; Moosmüller, H.; Chakrabarty, R. K.; Carrico, C. M.; Kreidenweis, S.
977 M.; Day, D. E.; Malm, W. C.; Laskin, A.; Jimenez, J. L.; Ulbrich, I. M.; Huffman, J. A.; Onasch, T.
978 B.; Trimborn, A.; Liu, L.; Mishchenko, M. I. Reduction in Biomass Burning Aerosol Light
979 Absorption upon Humidification: Roles of Inorganically-Induced Hygroscopicity, Particle Collapse,
980 and Photoacoustic Heat and Mass Transfer. *Atmos. Chem. Phys.* **2009**, *9* (22), 8949–8966 DOI:
981 10.5194/acp-9-8949-2009.

982 (20) Garofalo, L. A.; Pothier, M. A.; Levin, E. J. T.; Campos, T.; Kreidenweis, S. M.; Farmer, D. K.
983 Emission and Evolution of Submicron Organic Aerosol in Smoke from Wildfires in the Western
984 United States. *ACS Earth Space Chem.* **2019** DOI: 10.1021/acsearthspacechem.9b00125.

985 (21) Huffman, J. A.; Docherty, K. S.; Mohr, C.; Cubison, M. J.; Ulbrich, I. M.; Ziemann, P. J.; Onasch, T.
986 B.; Jimenez, J. L. Chemically-Resolved Volatility Measurements of Organic Aerosol from Different
987 Sources. *Environ. Sci. Technol.* **2009**, *43* (14), 5351–5357 DOI: 10.1021/es803539d.

988 (22) May, A. A.; Levin, E. J. T.; Hennigan, C. J.; Riipinen, I.; Lee, T.; Collett, J. L., Jr; Jimenez, J. L.;
989 Kreidenweis, S. M.; Robinson, A. L. Gas-Particle Partitioning of Primary Organic Aerosol
990 Emissions: 3. Biomass Burning. *J. Geophys. Res. D: Atmos.* **2013**, *118* (19) DOI:
991 10.1002/jgrd.50828.

992 (23) Hatch, L. E.; Rivas-Ubach, A.; Jen, C. N.; Lipton, M.; Goldstein, A. H.; Barsanti, K. C.
993 Measurements of I/SVOCs in Biomass-Burning Smoke Using Solid-Phase Extraction Disks and
994 Two-Dimensional Gas Chromatography. *Atmos. Chem. Phys.* **2018**, *18* (24), 17801–17817 DOI:
995 10.5194/acp-18-17801-2018.

996 (24) Hennigan, C. J.; Sullivan, A. P.; Collett, J. L., Jr; Robinson, A. L. Levoglucosan Stability in Biomass
997 Burning Particles Exposed to Hydroxyl Radicals: Levoglucosan Stability In Aerosol. *Geophys. Res.*
998 *Lett.* **2010**, *37* (9) DOI: 10.1029/2010gl043088.

999 (25) Jen, C. N.; Hatch, L. E.; Selimovic, V.; Yokelson, R. J.; Weber, R.; Fernandez, A. E.; Kreisberg, N.
1000 M.; Barsanti, K. C.; Goldstein, A. H. Speciated and Total Emission Factors of Particulate Organics

1001 from Burning Western US Wildland Fuels and Their Dependence on Combustion Efficiency. *Atmos.*
1002 *Chem. Phys.* **2019**, *19* (2), 1013–1026 DOI: 10.5194/acp-19-1013-2019.

1003 (26) Smith, J. D.; Sio, V.; Yu, L.; Zhang, Q.; Anastasio, C. Secondary Organic Aerosol Production from
1004 Aqueous Reactions of Atmospheric Phenols with an Organic Triplet Excited State. *Environ. Sci.*
1005 *Technol.* **2014**, *48* (2), 1049–1057 DOI: 10.1021/es4045715.

1006 (27) Hatch, L. E.; Yokelson, R. J.; Stockwell, C. E.; Veres, P. R.; Simpson, I. J.; Blake, D. R.; Orlando, J.
1007 J.; Barsanti, K. C. Multi-Instrument Comparison and Compilation of Non-Methane Organic Gas
1008 Emissions from Biomass Burning and Implications for Smoke-Derived Secondary Organic Aerosol
1009 Precursors. *Atmos. Chem. Phys.* **2017**, *17* (2), 1471–1489 DOI: 10.5194/acp-17-1471-2017.

1010 (28) Koss, A. R.; Sekimoto, K.; Gilman, J. B.; Selimovic, V.; Coggon, M. M.; Zarzana, K. J.; Yuan, B.;
1011 Lerner, B. M.; Brown, S. S.; Jimenez, J. L.; Krechmer, J.; Roberts, J. M.; Warneke, C.; Yokelson, R.
1012 J.; Gouw, J. de. Non-Methane Organic Gas Emissions from Biomass Burning: Identification,
1013 Quantification, and Emission Factors from PTR-ToF during the FIREX 2016 Laboratory
1014 Experiment. *Atmos. Chem. Phys.* **2018**, *18* (5), 3299–3319 DOI: 10.5194/acp-18-3299-2018.

1015 (29) Jathar, S. H.; Gordon, T. D.; Hennigan, C. J.; Pye, H. O. T.; Pouliot, G.; Adams, P. J.; Donahue, N.
1016 M.; Robinson, A. L. Unspeciated Organic Emissions from Combustion Sources and Their Influence
1017 on the Secondary Organic Aerosol Budget in the United States. *Proc. Natl. Acad. Sci. U. S. A.* **2014**,
1018 *111* (29), 10473–10478 DOI: 10.1073/pnas.1323740111.

1019 (30) Stockwell, C. E.; Veres, P. R.; Williams, J.; Yokelson, R. J. Characterization of Biomass Burning
1020 Emissions from Cooking Fires, Peat, Crop Residue, and Other Fuels with High-Resolution Proton-
1021 Transfer-Reaction Time-of-Flight Mass Spectrometry. *Atmos. Chem. Phys.* **2015**, *15* (2), 845–865
1022 DOI: 10.5194/acp-15-845-2015.

1023 (31) Hatch, L. E.; Luo, W.; Pankow, J. F.; Yokelson, R. J.; Stockwell, C. E.; Barsanti, K. C. Identification
1024 and Quantification of Gaseous Organic Compounds Emitted from Biomass Burning Using Two-
1025 Dimensional Gas Chromatography–time-of-Flight Mass Spectrometry. *Atmos. Chem. Phys.* **2015**, *15*
1026 (4), 1865–1899 DOI: 10.5194/acp-15-1865-2015.

1027 (32) Sekimoto, K.; Koss, A. R.; Gilman, J. B.; Selimovic, V.; Coggon, M. M.; Zarzana, K. J.; Yuan, B.;
1028 Lerner, B. M.; Brown, S. S.; Warneke, C.; Yokelson, R. J.; Roberts, J. M.; de Gouw, J. A. High- and
1029 Low-Temperature Pyrolysis Profiles Describe Volatile Organic Compound Emissions from Western
1030 US Wildfire Fuels. *Atmos. Chem. Phys.* **2018**, *18* (13) DOI: 10.5194/acp-18-9263-2018.

1031 (33) Palm, B. B.; Peng, Q.; Fredrickson, C. D.; Lee, B. H.; Garofalo, L. A.; Pothier, M. A.; Kreidenweis,
1032 S. M.; Farmer, D. K.; Pokhrel, R. P.; Shen, Y.; Murphy, S. M.; Permar, W.; Hu, L.; Campos, T. L.;
1033 Hall, S. R.; Ullmann, K.; Zhang, X.; Flocke, F.; Fischer, E. V.; Thornton, J. A. Quantification of
1034 Organic Aerosol and Brown Carbon Evolution in Fresh Wildfire Plumes. *Proc. Natl. Acad. Sci. U. S.
1035 A.* **2020**, *117* (47), 29469–29477 DOI: 10.1073/pnas.2012218117.

1036 (34) Permar, W.; Wang, Q.; Selimovic, V.; Wielgasz, C.; Yokelson, R. J.; Hornbrook, R. S.; Hills, A. J.;
1037 Apel, E. C.; Ku, I.-T.; Zhou, Y.; Sive, B. C.; Sullivan, A. P.; Collett, J. L., Jr; Campos, T. L.; Palm,
1038 B. B.; Peng, Q.; Thornton, J. A.; Garofalo, L. A.; Farmer, D. K.; Kreidenweis, S. M.; Levin, E. J. T.;
1039 DeMott, P. J.; Flocke, F.; Fischer, E. V.; Hu, L. Emissions of Trace Organic Gases from Western
1040 U.S. Wildfires Based on WE-CAN Aircraft Measurements. *J. Geophys. Res.* **2021**, *126* (11) DOI:
1041 10.1029/2020jd033838.

1042 (35) Bruns, E. A.; Slowik, J. G.; El Haddad, I.; Kilic, D.; Klein, F.; Dommen, J.; Temime-Roussel, B.;
1043 Marchand, N.; Baltensperger, U.; Prévôt, A. S. H. Characterization of Gas-Phase Organics Using
1044 Proton Transfer Reaction Time-of-Flight Mass Spectrometry: Fresh and Aged Residential Wood
1045 Combustion Emissions. *Atmos. Chem. Phys.* **2017**, *17* (1), 705–720 DOI: 10.5194/acp-17-705-2017.

1046 (36) Stefenelli, G.; Jiang, J.; Bertrand, A.; Bruns, E. A.; Pieber, S. M.; Baltensperger, U.; Marchand, N.;
1047 Aksoyoglu, S.; Prévôt, A. S. H.; Slowik, J. G.; Haddad, I. E. Secondary Organic Aerosol Formation
1048 from Smoldering and Flaming Combustion of Biomass: A Box Model Parametrization Based on
1049 Volatility Basis Set. *Atmos. Chem. Phys.* **2019**, *19* (17), 11461–11484 DOI: 10.5194/acp-19-11461-
1050 2019.

1051 (37) Ahern, A. T.; Robinson, E. S.; Tkacik, D. S.; Saleh, R.; Hatch, L. E.; Barsanti, K. C.; Stockwell, C.



1052 E.; Yokelson, R. J.; Presto, A. A.; Robinson, A. L.; Sullivan, R. C.; Donahue, N. M. Production of
 1053 Secondary Organic Aerosol During Aging of Biomass Burning Smoke From Fresh Fuels and Its
 1054 Relationship to VOC Precursors. *J. Geophys. Res. D: Atmos.* **2019**, *124* (6), 3583–3606 DOI:
 1055 10.1029/2018JD029068.

1056 (38) Akherati, A.; He, Y.; Coggon, M. M.; Koss, A. R.; Hodshire, A. L.; Sekimoto, K.; Warneke, C.; de
 1057 Gouw, J.; Yee, L.; Seinfeld, J. H.; Onasch, T. B.; Herndon, S. C.; Knighton, W. B.; Cappa, C. D.;
 1058 Kleeman, M. J.; Lim, C. Y.; Kroll, J. H.; Pierce, J. R.; Jathar, S. H. Oxygenated Aromatic
 1059 Compounds Are Important Precursors of Secondary Organic Aerosol in Biomass-Burning
 1060 Emissions. *Environ. Sci. Technol.* **2020** DOI: 10.1021/acs.est.0c01345.

1061 (39) Lim, C. Y.; Hagan, D. H.; Coggon, M. M.; Koss, A. R.; Sekimoto, K.; de Gouw, J.; Warneke, C.;
 1062 Cappa, C. D.; Kroll, J. H. Secondary Organic Aerosol Formation from the Laboratory Oxidation of
 1063 Biomass Burning Emissions. *Atmos. Chem. Phys.* **2019**, *19* (19), 12797–12809 DOI: 10.5194/acp-
 1064 19-12797-2019.

1065 (40) Hodshire, A. L.; Akherati, A.; Alvarado, M. J.; Brown-Steiner, B.; Jathar, S. H.; Jimenez, J. L.;
 1066 Kreidenweis, S. M.; Lonsdale, C. R.; Onasch, T. B.; Ortega, A. M.; Pierce, J. R. Aging Effects on
 1067 Biomass Burning Aerosol Mass and Composition: A Critical Review of Field and Laboratory
 1068 Studies. *Environ. Sci. Technol.* **2019**, *53* (17), 10007–10022 DOI: 10.1021/acs.est.9b02588.

1069 (41) Hennigan, C. J.; Miracolo, M. A.; Engelhart, G. J.; May, A. A.; Presto, A. A.; Lee, T.; Sullivan, A.
 1070 P.; McMeeking, G. R.; Coe, H.; Wold, C. E.; Hao, W.-M.; Gilman, J. B.; Kuster, W. C.; Gouw, J.
 1071 de; Schichtel, B. A.; Collett, J. L., Jr.; Kreidenweis, S. M.; Robinson, A. L. Chemical and Physical
 1072 Transformations of Organic Aerosol from the Photo-Oxidation of Open Biomass Burning Emissions
 1073 in an Environmental Chamber. *Atmos. Chem. Phys.* **2011**, *11* (15), 7669–7686 DOI: 10.5194/acp-11-
 1074 7669-2011.

1075 (42) Ortega, A. M.; Day, D. A.; Cubison, M. J.; Brune, W. H.; Bon, D.; de Gouw, J. A.; Jimenez, J. L.
 1076 Secondary Organic Aerosol Formation and Primary Organic Aerosol Oxidation from Biomass-
 1077 Burning Smoke in a Flow Reactor during FLAME-3. *Atmos. Chem. Phys.* **2013**, *13* (22), 11551–
 1078 11571 DOI: 10.5194/acp-13-11551-2013.

1079 (43) Tkacik, D. S.; Robinson, E. S.; Ahern, A.; Saleh, R.; Stockwell, C.; Veres, P.; Simpson, I. J.;
 1080 Meinardi, S.; Blake, D. R.; Yokelson, R. J.; Presto, A. A.; Sullivan, R. C.; Donahue, N. M.;
 1081 Robinson, A. L. A Dual-Chamber Method for Quantifying the Effects of Atmospheric Perturbations
 1082 on Secondary Organic Aerosol Formation from Biomass Burning Emissions: Investigation of
 1083 Biomass Burning SOA. *J. Geophys. Res. D: Atmos.* **2017**, *122* (11), 6043–6058 DOI:
 1084 10.1002/2016JD025784.

1085 (44) Hobbs, P. V.; Sinha, P.; Yokelson, R. J.; Christian, T. J.; Blake, D. R.; Gao, S.; Kirchstetter, T. W.;
 1086 Novakov, T.; Pilewskie, P. Evolution of Gases and Particles from a Savanna Fire in South Africa. *J.
 1087 Geophys. Res. D: Atmos.* **2003**, *108* (D13) DOI: 10.1029/2002JD002352.

1088 (45) Alvarado, M. J.; Prinn, R. G. Formation of Ozone and Growth of Aerosols in Young Smoke Plumes
 1089 from Biomass Burning: 1. Lagrangian Parcel Studies. *J. Geophys. Res.* **2009**, *114* (D9), D09307
 1090 DOI: 10.1029/2008JD011144.

1091 (46) Liu, J. C.; Mickley, L. J.; Sulprizio, M. P.; Dominici, F.; Yue, X.; Ebisu, K.; Anderson, G. B.; Khan,
 1092 R. F. A.; Bravo, M. A.; Bell, M. L. Particulate Air Pollution from Wildfires in the Western US under
 1093 Climate Change. *Clim. Change* **2016**, *138* (3), 655–666 DOI: 10.1007/s10584-016-1762-6.

1094 (47) DeCarlo, P. F.; Dunlea, E. J.; Kimmel, J. R.; Aiken, A. C.; Sueper, D.; Crounse, J.; Wennberg, P. O.;
 1095 Emmons, L.; Shinozuka, Y.; Clarke, A.; Zhou, J.; Tomlinson, J.; Collins, D. R.; Knapp, D.;
 1096 Weinheimer, A. J.; Montzka, D. D.; Campos, T.; Jimenez, J. L. Fast Airborne Aerosol Size and
 1097 Chemistry Measurements above Mexico City and Central Mexico during the MILAGRO Campaign.
 1098 *Atmos. Chem. Phys.* **2008**, *8* (14), 4027–4048 DOI: 10.5194/acp-8-4027-2008.

1099 (48) Yokelson, R. J.; Crounse, J. D.; DeCarlo, P. F.; Karl, T.; Urbanski, S.; Atlas, E.; Campos, T.;
 1100 Shinozuka, Y.; Kapustin, V.; Clarke, A. D.; Weinheimer, A.; Knapp, D. J.; Montzka, D. D.;
 1101 Holloway, J.; Weibring, P.; Flocke, F.; Zheng, W.; Toohey, D.; Wennberg, P. O.; Wiedinmyer, C.;
 1102 Mauldin, L.; Fried, A.; Richter, D.; Walega, J.; Jimenez, J. L.; Adachi, K.; Buseck, P. R.; Hall, S. R.;



1103 Shetter, R. Emissions from Biomass Burning in the Yucatan. *Atmos. Chem. Phys.* **2009**, *9* (15),
1104 5785–5812 DOI: 10.5194/acp-9-5785-2009.

1105 (49) Jolleys, M. D.; Coe, H.; McFiggans, G.; Capes, G.; Allan, J. D.; Crosier, J.; Williams, P. I.; Allen,
1106 G.; Bower, K. N.; Jimenez, J. L.; Russell, L. M.; Grutter, M.; Baumgardner, D. Characterizing the
1107 Aging of Biomass Burning Organic Aerosol by Use of Mixing Ratios: A Meta-Analysis of Four
1108 Regions. *Environ. Sci. Technol.* **2012**, *46* (24), 13093–13102 DOI: 10.1021/es302386v.

1109 (50) Vakkari, V.; Kerminen, V.-M.; Beukes, J. P.; Tiitta, P.; van Zyl, P. G.; Josipovic, M.; Venter, A. D.;
1110 Jaars, K.; Worsnop, D. R.; Kulmala, M.; Laakso, L. Rapid Changes in Biomass Burning Aerosols by
1111 Atmospheric Oxidation. *Geophys. Res. Lett.* **2014**, *41* (7), 2644–2651 DOI:
1112 10.1002/2014GL059396.

1113 (51) Vakkari, V.; Beukes, J. P.; Dal Maso, M.; Aurela, M.; Josipovic, M.; van Zyl, P. G. Major
1114 Secondary Aerosol Formation in Southern African Open Biomass Burning Plumes. *Nat. Geosci.*
1115 **2018**, *11* (8), 580–583 DOI: 10.1038/s41561-018-0170-0.

1116 (52) May, A. A.; Lee, T.; McMeeking, G. R.; Akagi, S.; Sullivan, A. P.; Urbanski, S.; Yokelson, R. J.;
1117 Kreidenweis, S. M. Observations and Analysis of Organic Aerosol Evolution in Some Prescribed
1118 Fire Smoke Plumes. *Atmos. Chem. Phys.* **2015**, *15* (11), 6323–6335 DOI: 10.5194/acp-15-6323-
1119 2015.

1120 (53) Akagi, S. K.; Craven, J. S.; Taylor, J. W.; McMeeking, G. R.; Yokelson, R. J.; Burling, I. R.;
1121 Urbanski, S. P.; Wold, C. E.; Seinfeld, J. H.; Coe, H.; Alvarado, M. J.; Weise, D. R. Evolution of
1122 Trace Gases and Particles Emitted by a Chaparral Fire in California. *Atmos. Chem. Phys.* **2012**, *12*
1123 (3), 1397–1421 DOI: 10.5194/acp-12-1397-2012.

1124 (54) Cubison, M. J.; Ortega, A. M.; Hayes, P. L.; Farmer, D. K.; Day, D.; Lechner, M. J.; Brune, W. H.;
1125 Apel, E.; Diskin, G. S.; Fisher, J. A.; Fuelberg, H. E.; Hecobian, A.; Knapp, D. J.; Mikoviny, T.;
1126 Riemer, D.; Sachse, G. W.; Sessions, W.; Weber, R. J.; Weinheimer, A. J.; Wisthaler, A.; Jimenez, J.
1127 L. Effects of Aging on Organic Aerosol from Open Biomass Burning Smoke in Aircraft and
1128 Laboratory Studies. *Atmos. Chem. Phys.* **2011**, *11* (23), 12049–12064 DOI: 10.5194/acp-11-12049-
1129 2011.

1130 (55) Brito, J.; Rizzo, L. V.; Morgan, W. T.; Coe, H.; Johnson, B.; Haywood, J.; Longo, K.; Freitas, S.;
1131 Andreae, M. O.; Artaxo, P. Ground-Based Aerosol Characterization during the South American
1132 Biomass Burning Analysis (SAMBBA) Field Experiment. *Atmos. Chem. Phys.* **2014**, *14* (22),
1133 12069–12083 DOI: 10.5194/acp-14-12069-2014.

1134 (56) Morgan, W. T.; Allan, J. D.; Bauguitte, S.; Darbyshire, E.; Flynn, M. J.; Lee, J.; Liu, D.; Johnson,
1135 B.; Haywood, J.; Longo, K. M.; Artaxo, P. E.; Coe, H. Transformation and Ageing of Biomass
1136 Burning Carbonaceous Aerosol over Tropical South America from Aircraft In Situ Measurements
1137 during SAMBBA. *Atmos. Chem. Phys.* **2020**, *20* (9), 5309–5326 DOI: 10.5194/acp-20-5309-2020.

1138 (57) Forrister, H.; Liu, J.; Scheuer, E.; Dibb, J.; Ziamba, L.; Thornhill, K. L.; Anderson, B.; Diskin, G.;
1139 Perring, A. E.; Schwarz, J. P.; Campuzano-Jost, P.; Day, D. A.; Palm, B. B.; Jimenez, J. L.; Nenes,
1140 A.; Weber, R. J. Evolution of Brown Carbon in Wildfire Plumes. *Geophys. Res. Lett.* **2015**, *42* (11),
1141 4623–4630 DOI: 10.1002/2015GL063897.

1142 (58) Collier, S.; Zhou, S.; Onasch, T. B.; Jaffe, D. A.; Kleinman, L.; Sedlacek, A. J., 3rd; Briggs, N. L.;
1143 Hee, J.; Fortner, E.; Shilling, J. E.; Worsnop, D.; Yokelson, R. J.; Parworth, C.; Ge, X.; Xu, J.;
1144 Butterfield, Z.; Chand, D.; Dubey, M. K.; Pekour, M. S.; Springston, S.; Zhang, Q. Regional
1145 Influence of Aerosol Emissions from Wildfires Driven by Combustion Efficiency: Insights from the
1146 BBOP Campaign. *Environ. Sci. Technol.* **2016**, *50* (16), 8613–8622 DOI: 10.1021/acs.est.6b01617.

1147 (59) Capes, G.; Johnson, B.; McFiggans, G.; Williams, P. I.; Haywood, J.; Coe, H. Aging of Biomass
1148 Burning Aerosols over West Africa: Aircraft Measurements of Chemical Composition,
1149 Microphysical Properties, and Emission Ratios. *J. Geophys. Res. D: Atmos.* **2008**, *113* (D23) DOI:
1150 10.1029/2008JD009845.

1151 (60) Jolleys, M. D.; Coe, H.; McFiggans, G.; Taylor, J. W.; O’Shea, S. J.; Le Breton, M.; Bauguitte, S. J.-
1152 B.; Moller, S.; Di Carlo, P.; Aruffo, E.; Palmer, P. I.; Lee, J. D.; Percival, C. J.; Gallagher, M. W.
1153 Properties and Evolution of Biomass Burning Organic Aerosol from Canadian Boreal Forest Fires.



1154 *Atmos. Chem. Phys.* **2015**, *15* (6), 3077–3095 DOI: 10.5194/acp-15-3077-2015.

1155 (61) Ng, N. L.; Canagaratna, M. R.; Jimenez, J. L.; Chhabra, P. S.; Seinfeld, J. H.; Worsnop, D. R.

1156 Changes in Organic Aerosol Composition with Aging Inferred from Aerosol Mass Spectra. *Atmos.*

1157 *Chem. Phys.* **2011**, *11* (13), 6465–6474 DOI: 10.5194/acp-11-6465-2011.

1158 (62) Bian, Q.; Jathar, S. H.; Kodros, J. K.; Barsanti, K. C.; Hatch, L. E.; May, A. A.; Kreidenweis, S. M.;

1159 Pierce, J. R. Secondary Organic Aerosol Formation in Biomass-Burning Plumes: Theoretical

1160 Analysis of Lab Studies and Ambient Plumes. *Atmos. Chem. Phys.* **2017**, *17* (8), 5459–5475 DOI:

1161 10.5194/acp-17-5459-2017.

1162 (63) Hodshire, A. L.; Bian, Q.; Ramnarine, E.; Lonsdale, C. R.; Alvarado, M. J.; Kreidenweis, S. M.;

1163 Jathar, S. H.; Pierce, J. R. More Than Emissions and Chemistry: Fire Size, Dilution, and Background

1164 Aerosol Also Greatly Influence Near-Field Biomass Burning Aerosol Aging. *J. Geophys. Res. D: Atmos.* **2019**, *124* (10), 5589–5611 DOI: 10.1029/2018JD029674.

1165 (64) Matsunaga, A.; Ziemann, P. J. Gas-Wall Partitioning of Organic Compounds in a Teflon Film

1166 Chamber and Potential Effects on Reaction Product and Aerosol Yield Measurements. *Aerosol Sci.*

1167 *Technol.* **2010**, *44* (10), 881–892 DOI: 10.1080/02786826.2010.501044.

1168 (65) Zhang, X.; Cappa, C. D.; Jathar, S. H.; McVay, R. C.; Ensberg, J. J.; Kleeman, M. J.; Seinfeld, J. H.

1169 Influence of Vapor Wall Loss in Laboratory Chambers on Yields of Secondary Organic Aerosol.

1170 *Proc. Natl. Acad. Sci. U. S. A.* **2014**, *111* (16), 5802–5807 DOI: 10.1073/pnas.1404727111.

1171 (66) Krechmer, J. E.; Pagonis, D.; Ziemann, P. J.; Jimenez, J. L. Quantification of Gas-Wall Partitioning

1172 in Teflon Environmental Chambers Using Rapid Bursts of Low-Volatility Oxidized Species

1173 Generated in Situ. *Environ. Sci. Technol.* **2016**, *50* (11), 5757–5765 DOI: 10.1021/acs.est.6b00606.

1174 (67) Liang, Y.; Sengupta, D.; Campmier, M. J.; Lunderberg, D. M.; Apte, J. S.; Goldstein, A. H. Wildfire

1175 Smoke Impacts on Indoor Air Quality Assessed Using Crowdsourced Data in California. *Proc. Natl.*

1176 *Acad. Sci. U. S. A.* **2021**, *118* (36) DOI: 10.1073/pnas.2106478118.

1177 (68) Lindaas, J.; Pollack, I. B.; Garofalo, L. A.; Pothier, M. A.; Farmer, D. K.; Kreidenweis, S. M.;

1178 Campos, T. L.; Flocke, F.; Weinheimer, A. J.; Montzka, D. D.; Tyndall, G. S.; Palm, B. B.; Peng, Q.;

1179 Thornton, J. A.; Permar, W.; Wielgasz, C.; Hu, L.; Ottmar, R. D.; Restaino, J. C.; Hudak, A. T.; Ku,

1180 I.-T.; Zhou, Y.; Sive, B. C.; Sullivan, A.; Collett, J. L., Jr; Fischer, E. V. Emissions of Reactive

1181 Nitrogen from Western U.S. Wildfires during Summer 2018. *J. Geophys. Res.* **2021**, *126* (2) DOI:

1182 10.1029/2020jd032657.

1183 (69) Juncosa Calahorrano, J. F.; Lindaas, J.; O'Dell, K.; Palm, B. B.; Peng, Q.; Flocke, F.; Pollack, I. B.;

1184 Garofalo, L. A.; Farmer, D. K.; Pierce, J. R.; Collett, J. L., Jr.; Weinheimer, A.; Campos, T.;

1185 Hornbrook, R. S.; Hall, S. R.; Ullmann, K.; Pothier, M. A.; Apel, E. C.; Permar, W.; Hu, L.; Hills, A.

1186 J.; Montzka, D.; Tyndall, G.; Thornton, J. A.; Fischer, E. V. Daytime Oxidized Reactive Nitrogen

1187 Partitioning in Western U.S. Wildfire Smoke Plumes. *J. Geophys. Res.* **2021**, *126* (4) DOI:

1188 10.1029/2020jd033484.

1189 (70) Lebegue, B.; Schmidt, M.; Ramonet, M.; Wastine, B.; Yver Kwok, C.; Laurent, O.; Belviso, S.;

1190 Guemri, A.; Philippon, C.; Smith, J.; Conil, S. Comparison of Nitrous Oxide (N₂O) Analyzers for

1191 High-Precision Measurements of Atmospheric Mole Fractions. *Atmospheric Measurement*

1192 *Techniques* **2016**, *9* (3), 1221–1238 DOI: 10.5194/amt-9-1221-2016.

1193 (71) Kupc, A.; Williamson, C.; Wagner, N. L.; Richardson, M.; Brock, C. A. Modification, Calibration,

1194 and Performance of the Ultra-High Sensitivity Aerosol Spectrometer for Particle Size Distribution

1195 and Volatility Measurements during the Atmospheric Tomography Mission (ATom) Airborne

1196 Campaign. *Atmos. Meas. Tech.* **2018**, *11* (1), 369–383 DOI: 10.5194/amt-11-369-2018.

1197 (72) Hodshire, A. L.; Ramnarine, E.; Akherati, A.; Alvarado, M. L.; Farmer, D. K.; Jathar, S. H.;

1198 Kreidenweis, S. M.; Lonsdale, C. R.; Onasch, T. B.; Springston, S. R.; Wang, J.; Wang, Y.;

1199 Kleinman, L. I.; Sedlacek, A. J., III; Pierce, J. R. Dilution Impacts on Smoke Aging: Evidence in

1200 Biomass Burning Observation Project (BBOP) Data. *Atmos. Chem. Phys.* **2021**, *21* (9), 6839–6855

1201 DOI: 10.5194/acp-21-6839-2021.

1202 (73) Griffith, S. M.; Hansen, R. F.; Dusander, S.; Michoud, V.; Gilman, J. B.; Kuster, W. C.; Veres, P. R.;

1203 Graus, M.; de Gouw, J. A.; Roberts, J.; Young, C.; Washenfelder, R.; Brown, S. S.; Thalman, R.;

1204



1205 Waxman, E.; Volkamer, R.; Tsai, C.; Stutz, J.; Flynn, J. H.; Grossberg, N.; Lefer, B.; Alvarez, S. L.;
1206 Rappenglueck, B.; Mielke, L. H.; Osthoff, H. D.; Stevens, P. S. Measurements of Hydroxyl and
1207 Hydroperoxy Radicals during CalNex-LA: Model Comparisons and Radical Budgets. *J. Geophys. Res. D: Atmos.* **2016**, *121* (8), 4211–4232 DOI: 10.1002/2015JD024358.

1208 (74) Peng, Q.; Palm, B. B.; Melander, K. E.; Lee, B. H.; Hall, S. R.; Ullmann, K.; Campos, T.;
1209 Weinheimer, A. J.; Apel, E. C.; Hornbrook, R. S.; Hills, A. J.; Montzka, D. D.; Flocke, F.; Hu, L.;
1210 Permar, W.; Wielgasz, C.; Lindaas, J.; Pollack, I. B.; Fischer, E. V.; Bertram, T. H.; Thornton, J. A.
1211 HONO Emissions from Western U.S. Wildfires Provide Dominant Radical Source in Fresh Wildfire
1212 Smoke. *Environ. Sci. Technol.* **2020**, *54* (10), 5954–5963 DOI: 10.1021/acs.est.0c00126.

1213 (75) Cappa, C. D.; Wilson, K. R. Multi-Generation Gas-Phase Oxidation, Equilibrium Partitioning, and
1214 the Formation and Evolution of Secondary Organic Aerosol. *Atmos. Chem. Phys.* **2012**, *12* (20),
1215 9505–9528 DOI: 10.5194/acp-12-9505-2012.

1216 (76) Jathar, S. H.; Cappa, C. D.; Wexler, A. S.; Seinfeld, J. H.; Kleeman, M. J. Multi-Generational
1217 Oxidation Model to Simulate Secondary Organic Aerosol in a 3-D Air Quality Model. *Geoscientific
1218 Model Development* **2015**, *8* (8), 2553–2567 DOI: 10.5194/gmd-8-2553-2015.

1219 (77) Adams, P. J.; Seinfeld, J. H. Predicting Global Aerosol Size Distributions in General Circulation
1220 Models. *J. Geophys. Res. D: Atmos.* **2002**, *107* (D19), AAC 4–1 – AAC 4–23 DOI:
1221 10.1029/2001JD001010.

1222 (78) Pierce, J. R.; Riipinen, I.; Kulmala, M.; Ehn, M.; Petäjä, T.; Junninen, H.; Worsnop, D. R.; Donahue,
1223 N. M. Quantification of the Volatility of Secondary Organic Compounds in Ultrafine Particles
1224 during Nucleation Events. *Atmos. Chem. Phys.* **2011**, *11* (17), 9019–9036 DOI: 10.5194/acp-11-
1225 9019-2011.

1226 (79) Jathar, S. H.; Cappa, C. D.; Wexler, A. S.; Seinfeld, J. H.; Kleeman, M. J. Simulating Secondary
1227 Organic Aerosol in a Regional Air Quality Model Using the Statistical Oxidation Model -- Part 1:
1228 Assessing the Influence of Constrained Multi-Generational Ageing. *Atmos. Chem. Phys.* **2016**, *16*
1229 (4), 2309–2322 DOI: 10.5194/acp-16-2309-2016.

1230 (80) Eluri, S.; Cappa, C. D.; Friedman, B.; Farmer, D. K.; Jathar, S. H. Modeling the Formation and
1231 Composition of Secondary Organic Aerosol from Diesel Exhaust Using Parameterized and Semi-
1232 Explicit Chemistry and Thermodynamic Models. *Atmos. Chem. Phys.* **2018**, *18* (19), 13813–13838
1233 DOI: 10.5194/acp-18-13813-2018.

1234 (81) Akherati, A.; Cappa, C. D.; Kleeman, M. J.; Docherty, K. S.; Jimenez, J. L.; Griffith, S. M.;
1235 Dusander, S.; Stevens, P. S.; Jathar, S. H. Simulating Secondary Organic Aerosol in a Regional Air
1236 Quality Model Using the Statistical Oxidation Model – Part 3: Assessing the Influence of Semi-
1237 Volatile and Intermediate-Volatility Organic Compounds and NO_x. *Atmos. Chem. Phys.* **2019**, *19*
1238 (7), 4561–4594 DOI: 10.5194/acp-19-4561-2019.

1239 (82) Cappa, C. D.; Jathar, S. H.; Kleeman, M. J.; Docherty, K. S.; Jimenez, J. L.; Seinfeld, J. H.; Wexler,
1240 A. S. Simulating Secondary Organic Aerosol in a Regional Air Quality Model Using the Statistical
1241 Oxidation Model--Part 2: Assessing the Influence of Vapor Wall Losses. *Atmos. Chem. Phys.* **2016**,
1242 *16* (5), 3041–3059.

1243 (83) He, Y.; Akherati, A.; Nah, T.; Ng, N. L.; Garofalo, L. A.; Farmer, D. K.; Shiraiwa, M.; Zaveri, R.
1244 A.; Cappa, C. D.; Pierce, J. R.; Jathar, S. H. Particle Size Distribution Dynamics Can Help Constrain
1245 the Phase State of Secondary Organic Aerosol. *Environ. Sci. Technol.* **2021**, *55* (3), 1466–1476 DOI:
1246 10.1021/acs.est.0c05796.

1247 (84) Garofalo, L. A.; He, Y.; Jathar, S. H.; Pierce, J. R.; Fredrickson, C. D.; Palm, B. B.; Thornton, J. A.;
1248 Mahrt, F.; Crescenzo, G. V.; Bertram, A. K.; Draper, D. C.; Fry, J. L.; Orlando, J.; Zhang, X.;
1249 Farmer, D. K. Heterogeneous Nucleation Drives Particle Size Segregation in Sequential Ozone and
1250 Nitrate Radical Oxidation of Catechol. *Environ. Sci. Technol.*, *in review*.

1251 (85) He, Y.; King, B.; Pothier, M.; Lewane, L.; Akherati, A.; Mattila, J.; Farmer, D. K.; McCormick, R.
1252 L.; Thornton, M.; Pierce, J. R.; Volckens, J.; Jathar, S. H. Secondary Organic Aerosol Formation
1253 from Evaporated Biofuels: Comparison to Gasoline and Correction for Vapor Wall Losses. *Environ.
1254 Sci. Process. Impacts* **2020**, *22* (7), 1461–1474 DOI: 10.1039/d0em00103a.

1255



Open Access Article. Published on 15 June 2022. Downloaded on 7/2/2022 12:56:50 AM.
This article is licensed under a Creative Commons Attribution-NonCommercial 3.0 Unported Licence.


1256 (86) Zaveri, R. A.; Easter, R. C.; Shilling, J. E.; Seinfeld, J. H. Modeling Kinetic Partitioning of
1257 Secondary Organic Aerosol and Size Distribution Dynamics: Representing Effects of Volatility,
1258 Phase State, and Particle-Phase Reaction. *Atmos. Chem. Phys.* **2014**, *14* (10), 5153–5181 DOI:
1259 10.5194/acp-14-5153-2014.
1260 (87) Loza, C. L.; Craven, J. S.; Yee, L. D.; Coggon, M. M.; Schwantes, R. H.; Shiraiwa, M.; Zhang, X.;
1261 Schilling, K. A.; Ng, N. L.; Canagaratna, M. R.; Ziemann, P. J.; Flagan, R. C.; Seinfeld, J. H.
1262 Secondary Organic Aerosol Yields of 12-Carbon Alkanes. *Atmos. Chem. Phys.* **2014**, *14* (3), 1423–
1263 1439 DOI: 10.5194/acp-14-1423-2014.
1264 (88) Ng, N. L.; Kroll, J. H.; Chan, A. W. H.; Chhabra, P. S.; Flagan, R. C.; Seinfeld, J. H. Secondary
1265 Organic Aerosol Formation from m-Xylene, Toluene, and Benzene. *Atmos. Chem. Phys.* **2007**, *7*
1266 (14), 3909–3922 DOI: 10.5194/acp-7-3909-2007.
1267 (89) Yee, L. D.; Kautzman, K. E.; Loza, C. L.; Schilling, K. A.; Coggon, M. M.; Chhabra, P. S.; Chan,
1268 M. N.; Chan, A. W. H.; Hersey, S. P.; Crounse, J. D.; Wennberg, P. O.; Flagan, R. C.; Seinfeld, J. H.
1269 Secondary Organic Aerosol Formation from Biomass Burning Intermediates: Phenol and
1270 Methoxyphenols. *Atmos. Chem. Phys.* **2013**, *13* (16), 8019–8043 DOI: 10.5194/acp-13-8019-2013.
1271 (90) Chhabra, P. S.; Ng, N. L.; Canagaratna, M. R.; Corrigan, A. L.; Russell, L. M.; Worsnop, D. R.;
1272 Flagan, R. C.; Seinfeld, J. H. Elemental Composition and Oxidation of Chamber Organic Aerosol.
1273 *Atmos. Chem. Phys.* **2011**, *11* (17), 8827–8845 DOI: 10.5194/acp-11-8827-2011.
1274 (91) Grieshop, A. P.; Miracolo, M. A.; Donahue, N. M.; Robinson, A. L. Constraining the Volatility
1275 Distribution and Gas-Particle Partitioning of Combustion Aerosols Using Isothermal Dilution and
1276 Thermo denuder Measurements. *Environ. Sci. Technol.* **2009**, *43* (13), 4750–4756 DOI:
1277 10.1021/es8032378.
1278 (92) Huffman, J. A.; Docherty, K. S.; Aiken, A. C.; Cubison, M. J.; Ulbrich, I. M.; DeCarlo, P. F.;
1279 Sueper, D.; Jayne, J. T.; Worsnop, D. R.; Ziemann, P. J.; Jimenez, J. L. Chemically-Resolved
1280 Aerosol Volatility Measurements from Two Megacity Field Studies. *Atmos. Chem. Phys.* **2009**, *9*
1281 (18), 7161–7182 DOI: 10.5194/acp-9-7161-2009.
1282 (93) EPA. EPI SuiteTM-estimation program interface <https://www.epa.gov/tsca-screening-tools/epi-suitetm-estimation-program-interface> (accessed Mar 20, 2021).
1283 (94) Stewart, G. J.; Nelson, B. S.; Acton, W. J. F.; Vaughan, A. R.; Farren, N. J.; Hopkins, J. R.; Ward,
1284 M. W.; Swift, S. J.; Arya, R.; Mondal, A.; Jangirh, R.; Ahlawat, S.; Yadav, L.; Sharma, S. K.;
1285 Yunus, S. S. M.; Hewitt, C. N.; Nemitz, E.; Mullinger, N.; Gadi, R.; Sahu, L. K.; Tripathi, N.;
1286 Rickard, A. R.; Lee, J. D.; Mandal, T. K.; Hamilton, J. F. Emissions of Intermediate-Volatility and
1287 Semi-Volatile Organic Compounds from Domestic Fuels Used in Delhi, India. *Atmos. Chem. Phys.*
1288 **2021**, *21* (4), 2407–2426 DOI: 10.5194/acp-21-2407-2021.
1289 (95) Joo, T.; Rivera-Rios, J. C.; Takeuchi, M.; Alvarado, M. J.; Ng, N. L. Secondary Organic Aerosol
1290 Formation from Reaction of 3-Methylfuran with Nitrate Radicals. *ACS Earth Space Chem.* **2019**, *3*
1291 (6), 922–934 DOI: 10.1021/acsearthspacechem.9b00068.
1292 (96) Lu, Q.; Zhao, Y.; Robinson, A. L. Comprehensive Organic Emission Profiles for Gasoline, Diesel,
1293 and Gas-Turbine Engines Including Intermediate and Semi-Volatile Organic Compound Emissions.
1294 *Atmos. Chem. Phys.* **2018**, *18* (23), 17637–17654 DOI: 10.5194/acp-18-17637-2018.
1295 (97) Chan, A. W. H.; Chan, M. N.; Surratt, J. D.; Chhabra, P. S.; Loza, C. L.; Crounse, J. D.; Yee, L. D.;
1296 Flagan, R. C.; Wennberg, P. O.; Seinfeld, J. H. Role of Aldehyde Chemistry and NO_x
1297 Concentrations in Secondary Organic Aerosol Formation. *Atmos. Chem. Phys.* **2010**, *10* (15), 7169–
1298 7188 DOI: 10.5194/acp-10-7169-2010.
1299 (98) Henry, K. M.; Donahue, N. M. Photochemical Aging of α -Pinene Secondary Organic Aerosol:
1300 Effects of OH Radical Sources and Photolysis. *J. Phys. Chem. A* **2012**, *116* (24), 5932–5940 DOI:
1301 10.1021/jp210288s.
1302 (99) Zawadowicz, M. A.; Lee, B. H.; Shrivastava, M.; Zelenyuk, A.; Zaveri, R. A.; Flynn, C.; Thornton,
1303 J. A.; Shilling, J. E. Photolysis Controls Atmospheric Budgets of Biogenic Secondary Organic
1304 Aerosol. *Environ. Sci. Technol.* **2020**, *54* (7), 3861–3870 DOI: 10.1021/acs.est.9b07051.
1305 (100) Huang, D. D.; Zhang, Q.; Cheung, H. H. Y.; Yu, L.; Zhou, S.; Anastasio, C.; Smith, J. D.; Chan,

1307 C. K. Formation and Evolution of aqSOA from Aqueous-Phase Reactions of Phenolic Carbonyls:
1308 Comparison between Ammonium Sulfate and Ammonium Nitrate Solutions. *Environ. Sci. Technol.*
1309 **2018**, *52* (16), 9215–9224 DOI: 10.1021/acs.est.8b03441.

1310 (101) Kleinman, L. I.; Sedlacek, A. J. *Biomass Burning Observation Project (BBOP) Final Campaign*
1311 *Report*; DOE/SC-ARM-15-083; DOE ARM Climate Research Facility, Washington, DC (United
1312 States), 2016.

1313 (102) Zuidema, P.; Alvarado, M.; Chiu, C.; de Szoke, S.; Fairall, C.; Feingold, G.; Freedman, A.;
1314 Ghan, S.; Haywood, J.; Kollas, P.; Lewis, E.; McFarquhar, G.; McComiskey, A.; Mechem, D.;
1315 Onasch, T.; Redemann, J.; Romps, D.; Turner, D.; Wang, H.; Wood, R.; Yuter, S.; Zhu, P. *Layered*
1316 *Atlantic Smoke Interactions with Clouds (LASIC) Field Campaign Report*; DOE/SC-ARM-18-018;
1317 DOE Office of Science Atmospheric Radiation Measurement (ARM) Program (United States), 2018.

